Plasma L-Cystine/L-Glutamate Imbalance Increases Tumor Necrosis Factor-Alpha from CD14+ Circulating Monocytes in Patients with Advanced Cirrhosis

Eiji Kakazu[1], Yoshiyuki Ueno[1]*, Yasuteru Kondo[1], Jun Inoue[1], Masashi Ninomiya[1], Osamu Kimura[1], Yuta Wakui[1], Koji Fukushima[1], Keiichi Tamai[2], Tooru Shimosegawa[1]

1 Division of Gastroenterology, Tohoku University Graduate School of Medicine, Aobaku, Sendai, Japan, **2** Miyagi Cancer Center, Natori, Japan

Abstract

Background and Aims: The innate immune cells can not normally respond to the pathogen in patients with decompensated cirrhosis. Previous studies reported that antigen-presenting cells take up L-Cystine (L-Cys) and secrete substantial amounts of L-Glutamate (L-Glu) via the transport system Xc- (4F2hc+xCT), and that this exchange influences the immune responses. The aim of this study is to investigate the influence of the plasma L-Cys/L-Glu imbalance observed in patients with advanced cirrhosis on the function of circulating monocytes.

Methods: We used a serum-free culture medium consistent with the average concentrations of plasma amino acids from patients with advanced cirrhosis (ACM), and examined the function of CD14+ monocytes or THP-1 under ACM that contained 0–300 nmol/mL L-Cys with LPS. In patients with advanced cirrhosis, we actually determined the TNF-alpha and xCT mRNA of monocytes, and evaluated the correlation between the plasma L-Cys/L-Glu ratio and TNF-alpha.

Results: The addition of L-Cys significantly increased the production of TNF alpha from monocytes under ACM. Monocytes with LPS and THP-1 expressed xCT and a high level of extracellular L-Cys enhanced L-Cys/L-Glu antiport, and the intracellular GSH/GSSG ratio was decreased. The L-Cys transport was inhibited by excess L-Glu. In patients with advanced cirrhosis (n = 19), the TNF-alpha and xCT mRNA of monocytes were increased according to the Child-Pugh grade. The TNF-alpha mRNA of monocytes was significantly higher in the high L-Cys/L-Glu ratio group than in the low ratio group, and the plasma TNF-alpha was significantly correlated with the L-Cys/L-Glu ratio.

Conclusions: A plasma L-Cys/L-Glu imbalance, which appears in patients with advanced cirrhosis, increased the TNF-alpha from circulating monocytes via increasing the intracellular oxidative stress. These results may reflect the immune abnormality that appears in patients with decompensated cirrhosis.

Citation: Kakazu E, Ueno Y, Kondo Y, Inoue J, Ninomiya M, et al. (2011) Plasma L-Cystine/L-Glutamate Imbalance Increases Tumor Necrosis Factor-Alpha from CD14+ Circulating Monocytes in Patients with Advanced Cirrhosis. PLoS ONE 6(8): e23402. doi:10.1371/journal.pone.0023402

Editor: Stefan Bereswill, Charité-University Medicine Berlin, Germany

Received June 27, 2011; **Accepted** July 15, 2011; **Published** August 17, 2011

Funding: This study was supported in part by a grant-in-aid from the Ministry of Education, Culture, Sports, Science, and Technology of Japan to EK (23790762), and by Health and Labour Sciences Research Grants for the Research on Measures for Intractable Diseases (from the Ministry of Health, Labour and Welfare of Japan) to YU. The funders had no role in study design, data collection and analysis, decision to publish, or preparation of the manuscript.

Competing Interests: The authors have declared that no competing interests exist.

* E-mail: yueno@med.tohoku.ac.jp

Introduction

Circulating levels of proinflammatory cytokines such as TNF-alpha, IL-1 beta and IL-6 are increased in patients with cirrhosis [1,2,3]. Endotoxemia has been assumed to be responsible for the increased of such cytokines in patients with cirrhosis [4], because the activation of monocytes, macrophages and dendritc cells (DCs) by lipopolysaccharide (LPS) plays a key role in the pathogenesis of cytokine overproduction. This overproduction of proinflammatory cytokines leads to various complications, such as spontaneous bacterial peritonitis (SBP) and hepatorenal syndrome (HRS) in patients with advanced cirrhosis [5,6].

On the other hand, various types of amino acid imbalance appear in the plasma of patients with decompensated cirrhosis, since the liver plays a major role in metabolism involving glucose, lipids, vitamins,minerals and amino acids. An imbalance of plasma amino acids, with decreased levels of branched-chain amino acids (BCAAs) and increased levels of aromatic amino acids (AAAs), is commonly seen in patients with advanced cirrhosis [7]. Previously, we reported that extracellular branched-chain amino acids (BCAAs) regulate the maturation and function of monocyte derived dendritic cells [8], and that the addition of branched chain amino acids enhances the maturation and function of myeloid dendritic cells ex vivo in patients with advanced cirrhosis [9]. However, it is not clear whether the imbalance of amino acids other than BCAAs influence the immune responses in patients with advanced cirrhosis. A previous study showed that the concentration of plasma L- Cystine (L-Cys) is higher in patients with cirrhosis and shows a wide range of variation [10]. Increased levels of L-Glutamine (L-Gln) and decreasing levels of

L-Glutamate (L-Glu) are seen in patients with advanced cirrhosis, because the L-Glu-L-Gln exchange regulates the high levels of toxic ammonia in such patients [11]. Furthermore, previous studies demonstrated that antigen-presenting cells take up L-Cys via the Na-independent anionic amino acid transport system Xc^-(4F2hc+xCT) and secrete substantial amounts of L-Glu, influencing the immune-responses through this exchange [12,13,14]. This transporter is composed of two protein components, xCT and 4F2hc (CD98), and the transport activity is thought to be mediated by xCT [15,16]. The aim of this study is to investigate the influence of the extracellular L-Cys/L-Glu imbalance observed in patients with advanced cirrhosis on the function of peripheral monocytes using a serum-free culture medium with the average concentration of plasma amino acids from patients with advanced cirrhosis [9], thereby approximating the actual environment of the living body.

Materials and Methods

Ethics Statement

Written informed consent was obtained from each individual and the study protocol was approved by the Ethics Committee of Tohoku University School of Medicine (2009-209, 2009-535).

Monocyte count and isolation

In patients with cirrhosis, the monocyte and lymphocyte counts were measured by a Beckman Coulter LH 750 Analyzer (Fullerton, CA, USA). PBMCs were separated from the peripheral blood of healthy volunteers or patients with cirrhosis by centrifugation on a density gradient. The CD14-positive monocytes were isolated from PBMCs using magnetic microbeads (Miltenyi Biotec, Bergish Gladbach).

The serum free culture media used in this study

A serum free culture medium with the average concentration of plasma amino acids from healthy volunteers (HCM), that from patients with advanced cirrhosis (ACM) and complete culture media (CCM) were described previously [9]. Other components except amino acids were identical among media. Various concentrations of L-Cys were added to L-Cys free ACM , and the final concentration was adjusted to 0–300 nmol/mL (Table S1). We cultured CD14+monocytes, THP-1, Jurkat and Molt-4 under the these media with stimulant and measured the amino acid concentrations of these media. The viability of monocytes and PBMCs was determined using Annexin V^{FITC}, with dead cells identified by propidium iodide (PI) staining (Annexin V^{-FITC} Apoptosis Detection Kit, BioVision, Mountain View, CA), according to the manufacturer's instructions. We confirmed the viability of PBMCs cultured in ACM and ACM plus L-Cys to be equal to that of complete culture medium (CCM) and X-VIVO 10 (Cambrex Bio Science Walkersville, Inc. Walkersville, MD USA).

Patients and Healthy volunteers

The concentrations of the plasma amino acids from fasting patients with chronic hepatitis (n = 17), and patients with cirrhosis (n = 130) were measured by high-performance liquid

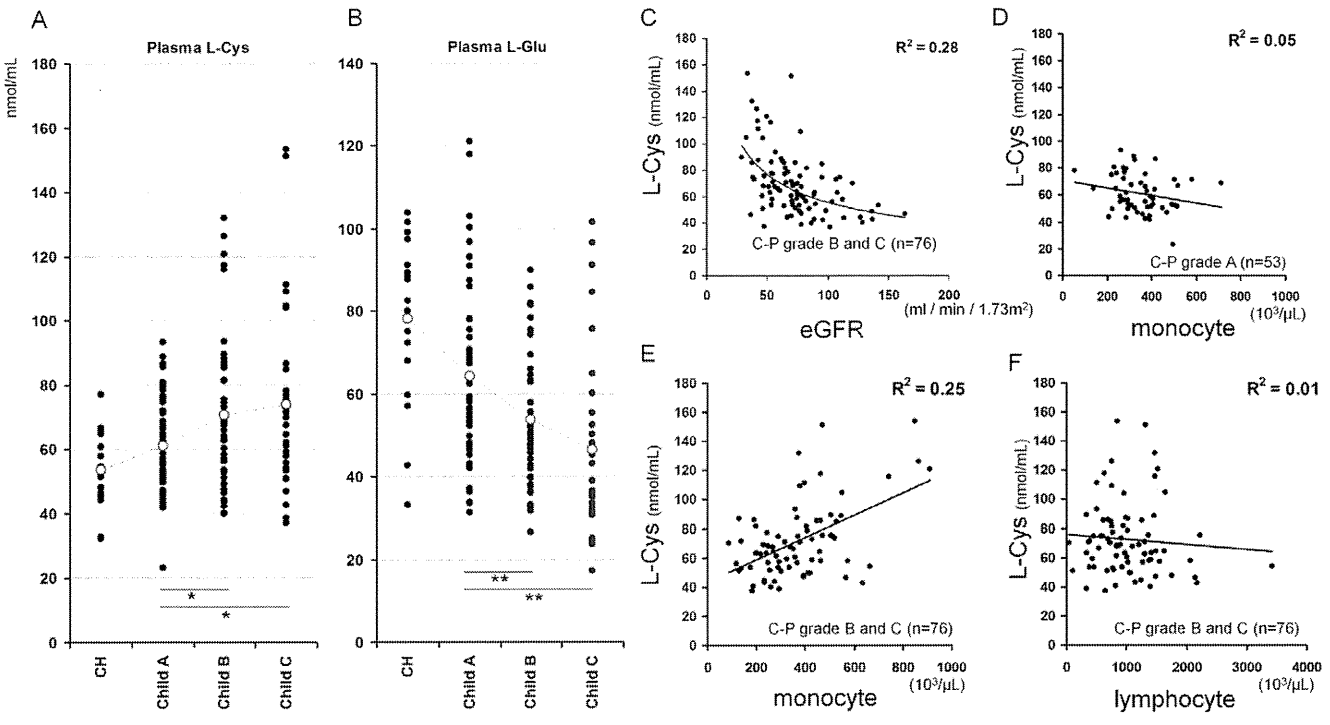

Figure 1. The counts of peripheral monocyte were increased in association with plasma L-Cystine in patients with advanced cirrhosis. A, B, The concentrations of plasma L-Cys in patients with cirrhosis was increased and that of plasma L-Glu was decreased acccording to Child-Pugh grade. The levels of plasma L-Cys and L-Glu in patients with cirrrhosis (n = 130) were measured using HPLC and classfied by the Child-Pugh classfication. C, Nonliner regression model was used to model variation in plasma L-Cys and eGFR. D, E,F, Linear regression model was used to model variation in plasma L-Cys and monocyte and lymphocyte counts. Individual correlations between plasma L-Cys levels and monocyte counts in patients with early cirrhosis (D), that in patients with advanced cirrhosis (E), and lymphocyte counts in patients with advanced cirrhosis (F). A,B, **, $p<0.01$, _*, $p<0.05$ vs Child-Pugh grade A. Statistical significance was determined by one-way ANOVA and Dunnett's post-hoc procedure. C, D, E, F, R^2 represents coefficient of determination.
doi:10.1371/journal.pone.0023402.g001

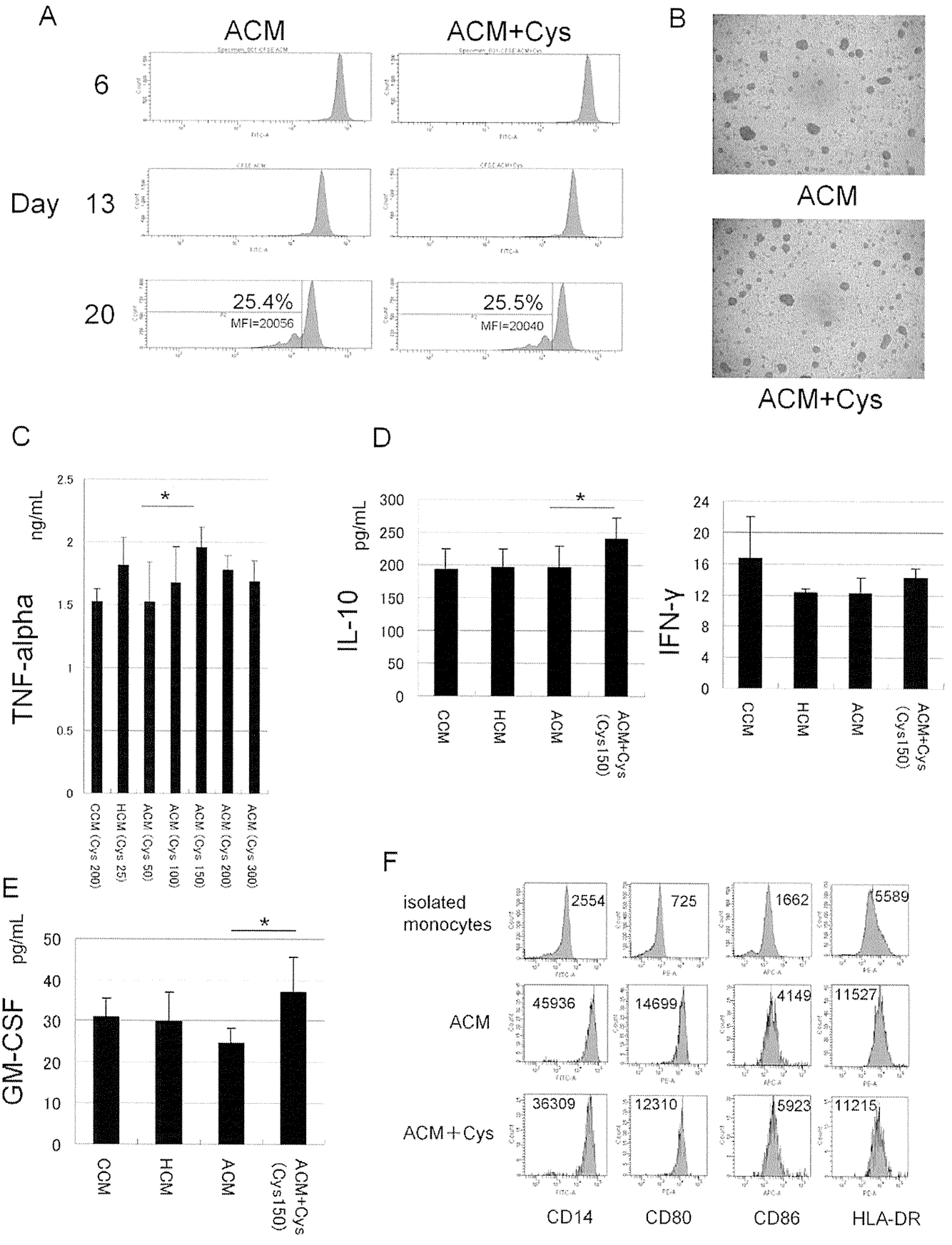
A
ACM
ACM+Cys
6
Day 13
20
25.4%
MFI=20056
25.5%
MFI=20040
B
ACM
ACM+Cys
C
TNF-alpha
ng/mL
CCM (Cys 200)
HCM (Cys 25)
ACM (Cys 50)
ACM (Cys 100)
ACM (Cys 150)
ACM (Cys 200)
ACM (Cys 300)
D
IL-10
pg/mL
IFN-γ
CCM
HCM
ACM
ACM+Cys (Cys150)
E
GM-CSF
pg/mL
F
isolated monocytes
ACM
ACM+Cys
2554
725
1662
5589
45936
14699
4149
11527
36309
12310
5923
11215
CD14
CD80
CD86
HLA-DR

Figure 2. L-Cystine dose-dependently increased TNF-alpha from CD14+ monocytes with LPS under the amino acid environment of patients with advanced cirrhosis. A, Isolated CD14+ monocytes (purity >90%) were cultured at a density of 2.5×10^5 cells/well in 96-well plates containing in ACM and ACM plus L-Cys (L-Cys : 150 nmol/mL) with 1,000 U/mL M-CSF. One half the amount of culture fluid was exchanged every one day. Cells were maintained for 20 days and the proliferation rate of the cells was measured using CFSE staining. B, Influence of L-Cys on microscopic appearance of monocyte proliferation under serum-free conditions. Day 20, cells in firmly adherent clusters in both ACM and ACM+Cys. C, Monocytes were cultured under CCM, HCM, ACM and ACM plus L-Cys (100–300 nmol/mL). Cells were pre-incubated at a density of 2.5×10^5 cells/well in 96-well flat-bottom plates for 2 hours in each of the media, and 100 ng/mL LPS was added. The supernatants were collected after 24 hours and immediately TNF-alpha was determined by specific cytokine ELISA kits. D,E, Similarly as in Fig. 2C, IL-10, IFN gamma from monocytes and GM-CSF from PBMCs under CCM, HCM, ACM, ACM+Cys (L-Cys 150 nmol/mL) were measured with ELISA. F, Cells were harvested after 24 hours, stained with different mAbs, and analyzed using flow cytometry. Cells were stained with FITC-labeled anti-CD14, -CD80, -CD86, and -HLA-DR. A, B and F results are representative of four experiments from three different donors. C, D and E, Mean ± SEM values from five different donors are shown. C,D,E *, $p<0.05$ vs ACM (paired Student's t test, two-tailed).
doi:10.1371/journal.pone.0023402.g002

chromatography (HPLC) in the early morning. Briefly, sulfosalicylic acid was added to the plasma to a final concentration of 5%. The samples were then placed on ice for 15 minutes followed by centrifugation to remove precipitated proteins. The extracts were then analyzed for the amino acid content with a JLC-500/V (Japan Electron Optics Laboratories, Tokyo, Japan). Also, the patients with cirrhosis were classified according to the Child-Pugh classification. We defined as Child-Pugh grade B or C the patients with advanced cirrhosis. The estimated glomerular filtration rate (eGFR) was calculated using the new Japanese equation [17].

We selected nineteen patients with cirrhosis for in vitro or ex vivo studies (Table S2). All of these patients were inpatients. The MELD score [18] was calculated by an on-line worksheet available on the internet at www.mayoclinic.org/meld/mayomodel5.html.

Monocyte proliferation assay

Monocytes were cultured at a density of 2.5×10^5 cells/well in 96-well plates containing each media with 1,000 U/mL M-CSF (PEPROTECH EC, London, UK). One half the amount of culture fluid was exchanged every one day. Cells were maintained for 20 days and the proliferation rate of the cells was measured using Carboxyfluorescein Succinimidyl Ester (CFSE) staining; CellTrace CFSE Cell Proliferation Kit (Molecular Probes, Oregon). The staining methods followed the manufacturer's protocol.

Cytokine analysis

PBMCs or monocytes were preincubated at a density of 2.5×10^5 cells/well in 96-well flat-bottom plates (CORNING, NY) for 2 hours in each of the media, and 100 ng/mL LPS (Escherichia coli 026:B6 (SIGMA) were added. The supernatants were collected after 24 hours and immediately TNF-alpha, IFN-gamma, IL-10, GM-CSF were determined by specific cytokine ELISA kits (Bender MedSystems) according to the manufacturer's instructions.

Surface marker analysis

Monocytes were harvested and labeled with FITC-, PE- and APC-labeled monoclonal antibodies (mAbs) (anti-human CD14, CD80, CD86, CD98, HLA-DR, or the relevant isotype controls: BD PharMingen, San Diego, CA), according to the manufacturer's instructions. On xCT expression, indirect staining was performed; primary antibody (xCT (H-121) scc-98552: Santa Cruz) secondary antibody (goat anti-rabbit IgG-FITC sc-2012: Santa Cruz) Using a FACS Canto II (BD Immunocytometry Systems, San Diego, CA) flow cytometer, surface marker expressions were analyzed using the BD FACSDiva (BD Immunocytometry Systems) program.

Intra-extracellular amino acid quantification

The THP-1, Jurkat and Molt4 cells were pre-incubated for 2 hr in ACM, then 1.0×10^7 cells were re-suspended with LPS (100 ng/mL) or IL-2 (1000 IU/mL) in 1 mL of ACM, L-Cys-free ACM or ACM with L-Cys. After 2 hr incubation, the supernatants were measured by HPLC for the extracellular amino acid quantification. The concentration of the intracellular amino acids was determined as described in ref [19]. Briefly, cells were washed two times by PBS and resuspended in 500 µL PBS sonicated with four 10-s pulses. Cell debris was removed by centrifugation, and sulfosalicylic acid was added to the supernatant to a final concentration of 2%. The samples were then placed on ice for 30 min followed by centrifugation to remove precipitated proteins. The extracts were then analyzed for amino acid content with an L-8500 amino acid analyzer (Hitachi Ltd., Tokyo).

Measurement of reduced glutathione (GSH) and oxidized glutathione (GSSG)

CD14+ monocytes were pre incubated at a density of 2.0×10^5 cells/well in 96-well plates containing HCM for 2 h and then cultured in HCM, ACM or ACM plus L-Cys for an additional 2 h. The culture medium was carefully removed from the wells. 100 µl of prepared GSH-Glo™ Reagent were added to each well of a 96-well plate, mixed briefly on a plate shaker, and incubated at room temperature for 30 minutes. 100 µl of reconstituted Luciferin Detection Reagent were added to each well of a 96-well plate, mixed briefly on a plate shaker, and incubated for 15 minutes. luminescence was read by a Lumino Skan Ascent (Thermo BioAnalysis, Helsinki, Finland).

Real-time PCR

THP-1, Jurkat, Molt-4 and CD14+ monocytes were collected. After the extraction of total RNA and the RT procedure, real-time PCR using aTaqMan Chemistry System () was carried out. The ready-made sets of primers and probes for the amplification of xCT (Assay ID : Hs00921937_m1), TNF-alpha (Assay ID : Hs99999043_m1) and glyceraldehyde-3-phosphate-dehydrogenase (GAPDH, Assay ID : Hs02758991_g1) were purchased from Perkin-Elmer/Applied Biosystems. The relative amount of target mRNA was obtained by using a comparative threshold cycle (CT) method. The expression level of mRNAs of the Molt-4 was represented as 1.0 and the relative amounts of target mRNA in THP-1 and Jurkat were calculated according to the manufacturer's protocol. For CD14+ monocytes, The expression level of monocyte mRNA from a healthy volunteer was represented as 1.0 and the relative amounts of target mRNA in monocytes from patients were calculated.

Statistical Analysis

The data were analyzed with ANOVA, and multiple comparisons were performed with Dunnett's post-hoc procedure for the plasma aminogram. When 2 groups were analyzed, the differences between media were analyzed by the Wilcoxon t test, and the

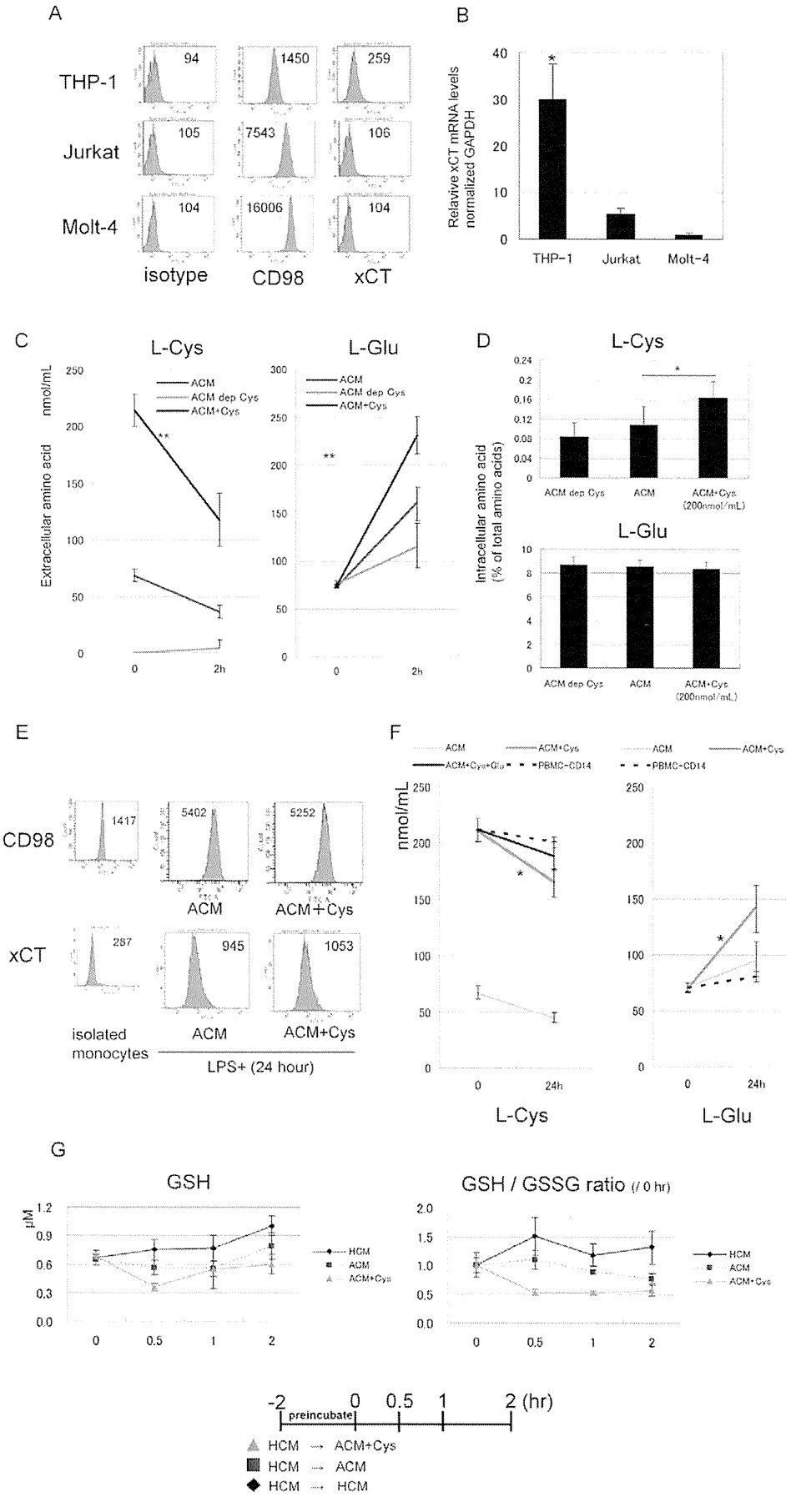
A
THP-1
Jurkat
Molt-4
94
1450
259
105
7543
106
104
16006
104
isotype
CD98
xCT
B
Relavive xCT mRNA levels normalized GAPDH
THP-1
Jurkat
Molt-4
C
L-Cys
L-Glu
nmol/mL
Extracellular amino acid
ACM
ACM dep Cys
ACM+Cys
D
L-Cys
L-Glu
Intracellular amino acid (% of total amino acids)
ACM dep Cys
ACM
ACM+Cys (200nmol/mL)
E
CD98
xCT
1417
5402
5252
287
945
1053
ACM
ACM+Cys
isolated monocytes
LPS+ (24 hour)
F
ACM
ACM+Cys
ACM+Cys+Glu
PBMC-CD14
nmol/mL
L-Cys
L-Glu
G
GSH
GSH / GSSG ratio (/ 0 hr)
μM
HCM
ACM
ACM+Cys
-2
preincubate
0
0.5
1
2 (hr)
HCM → ACM+Cys
HCM → ACM
HCM → HCM

Figure 3. High levels of extracellular L-Cystine promoted the L-Cystine-L-Glutamate antiport via xCT and decreased the intracellular GSH/GSSG ratio in monocyte under the amino acid environment of patients with advanced cirrhosis. A, THP-1, Jurkat and Molt-4 cultured under CCM were harvested and labeled with antibodies (CD98, xCT or the relevant isotype controls). Using flow cytometry, surface marker expressions were analyzed. The figure expresses the mean fluorescence intensity. Data shown are representative of three independent experiments with cells. B, xCT relative mRNA levels of these cell lines were determined by real time PCR: delta-delta CT method. All mRNA expression levels were normalized to GAPDH. C, D, The THP-1 cells were pre-incubated for 2 hours in ACM, then resusupended with LPS (100 ng/mL) in 1 mL of ACM, L-Cys-free ACM and ACM plus L-Cys. The concentration of extracellular (C) and intracellular (D) amino acid was determined as described in material and methods. E, The CD14+ monocytes, cultured under ACM and ACM plus L-Cys for 24 hours, were harvested and labeled with antibodies (CD98, xCT or the relevant isotype controls). Using flow cytometry, surface marker expressions were analyzed. The figure expresses the mean fluorescence Intensity. Data shown are representative of three independent experiments with cells. F, Similarly as in Fig. 4C, the monocytes were cultured for 24 hours in ACM, L-Cys-free ACM and ACM plus L-Cys. The supernatants were measured by HPLC as extracellular amino acids quantification. G, Monocytes were pre incubated at a density of 2.0×10^5 cells/well in 96-well flat-bottom plates for 2 hours in HCM, and then cultured in HCM, ACM and ACM plus L-Cys (200 nmol/mL) for an additional 2 hours. These intracellular glutathione levels were measured by GSH-Glo™ at the time point indicated. C and D, Mean ± SD values from five independent experiments are shown. B *, $p<0.05$ vs Molt-4 (the Mann-Whitney U-test.). C,F **, $p<0.01$ *,$P<0.05$ (mean change vs ACM) D *, $p<0.05$ (paired Student's t test, two-tailed).
doi:10.1371/journal.pone.0023402.g003

differences between healthy controls and patients were analyzed by the Mann-Whitney U-test. All statistical analyses were performed with standard statistical software (SPSS 13.0 for Windows, Chicago, IL).

Results

The counts of peripheral monocytes were increased in association with the plasma L-Cystine in patients with advanced cirrhosis

Firstly, we confirmed that, in patients with advanced cirrhosis (Child-Pugh grade B or C), the plasma concentrations of L-Cys were significantly higher than in those with early cirrhosis (Figure 1A), and there was a wide range of variation. On the other hand, the plasma concentrations of L-Glu were significantly decreased along with the Child-Pugh grade (Figure 1B). In patients with advanced cirrhosis, the wide range of variation of L-Cys was attributed to the eGFR ($R^2=0.28/P=0.0000008$) (Figure 1C). These data mean that plasma L-Cys increases in decompensated cirrhosis. Secondly, we investigate whether the concentration of plasma L-Cys influenced the peripheral monocyte counts. In patients with early cirrhosis, L-Cys was not correlated with the monocyte counts ($R^2=0.05/P=0.119$) (Figure 1D), but in patients with advanced cirrhosis, it was significantly and positively correlated with the monocyte counts ($R^2=0.25/P=0.0000017$) (Figure 1E). On the other hand, the lymphocyte counts were not correlated with the concentration of plasma L-Cys ($R^2=0.01/P=0.523$) (Figure 1F). Interestingly, among all twenty kinds of free amino acids, only L-Cys was significantly correlated with the monocyte counts in patients with advanced cirrhosis (Figure S1). These data mean that, in patients with advanced cirrhosis, plasma L-Cys is increased according to renal dysfunction and influences the counts of monocytes.

Extracellular L-Cystine dose-dependently increased pro-inflammatory cytokines from CD14+ monocytes under the amino acid condition of advanced cirrhosis

Based on the result that the peripheral monocyte counts were positively correlated with the concentration of L-Cys, we hypothesized that the concentration of extracellular L-Cys could influence the proliferation of monocytes. To investigate this hypothesis, we cultured monocytes for 20 days with M-CSF under ACM or ACM plus L-Cys in vitro, and determined the proliferation of monocytes by CFSE assay. An elevated concentration of L-Cys did not influence the proliferation of monocytes (Figure 2A) on microscopic appearance, and also did not affect the morphological appearance and behavior of the cells in culture (Figure 2B). There was also no difference in the proliferation of the monocyte cell line, THP-1 between these media (data not shown). Next, to investigate whether the extracellular L-Cys level influenced the production of inflammatory cytokines from monocytes, we cultured monocytes under ACM that contained 50–300 nmol/mL L-Cys and measured the producton of TNF alpha from monocytes. The addition of L-Cys increased the production of TNF alpha from monocytes in a dose-dependent manner (Figure 2C), and the values were maximum under 150 nmol/mL L-Cys. Interestingly, this range was in remarkable agreement with the range in patients with advanced cirrhosis (Fig. 1A). The IL-10 level from monocytes was also significantly higher under ACM plus L-Cys than that under ACM (Figure 2D), and there was no difference the interferon gamma (IFN γ) level from monocytes between these media. The GM-CSF from PBMCs was also significantly higher under ACM plus L-Cys than that under ACM (Figure 2E). Regarding monocyte phenotypes, there was no difference between ACM and ACM plus L-Cys (Figure 2F). These data mean that high levels of extracellular L-Cys increased pro-inflammatory cytokines from CD14+ monocytes under the amino acid environment of patients with advanced cirrhosis.

High levels of extracellular L-Cystine promoted the L-Cystine-L-Glutamate antiport and decreased the intracellular GSH/GSSG ratio in monocyte under the amino acid environment of patients with advanced cirrhosis

We investigated whether high levels of extracellular L-Cys influence the L-Cys/L-Glu transport under the amino acid environment of patients with advanced cirrhosis.

Firstly, we determined the expression of 4F2hc (CD98) and xCT in THP-1, Jurkat and Molt-4. All cell lines expressed CD98, but only THP-1 expressed xCT at the protein level (Fig. 3A) and mRNA level (Fig. 3B). Secondly, we measured the intra-extracellular L-Cys and L-Glu concentration of THP-1 under ACM at various L-Cys levels. After 2 hours culture, ACM plus L-Cys significantly decreased the extracellular L-Cys (mean change, ACM+Cys, −96.8±15.8; ACM, −32.3±0.6 and ACM dep L-Cys, 4.8±6.6 nmol/mL) (Fig. 3C) and significantly increased intracellular L-Cys (Fig. 3D) and extracellular L-Glu (mean change, ACM+Cys, 157.5±19; ACM, 86.1±17.7 and ACM dep L-Cys, 40.4±24.9 nmol/mL) (Fig. 3C) more than that by ACM or ACM deprived of L-Cys. For intracellular L-Glu, there was no difference among these media. Such L-Cys/L-Glu changes were not seen for Jurkat and Molt-4 (data not shown). These data indicate that high levels of extracellular L-Cys enhances L-Cys/L-Glu antiport in the monocyte cell line THP-1. Similarly, CD14+ monocytes expressed CD98 and xCT after adding LPS (Fig. 3E) and extracellular L-Cys/L-Glu changes were seen (L-Cys mean change, ACM+Cys, −46.9±5.0; ACM, −22.4±6.0; ACM+Cys+Glu, −22.9±6.4 and

PBMC-CD14, −11.0±11.9 nmol/mL/L-Glu mean change; ACM+Cys, 70.4±24.8; ACM, 25.2±13.8 and PBMC-CD14, 10.7±7.0 nmol/mL) (Fig. 3F). Furthermore, we investigated whether high levels of extracellular L-Cys influence the intracellular glutathione level of monocytes. Interestingly, the intracellular GSH and GSH/GSSG ratio decreased more under ACM plus L-Cys than under ACM or HCM (Fig. 3G).

Plasma L-Cys/L-Glu ratio significantly correlated with plasma TNF-alpha level in patients with advanced cirrhosis

Finally, we actually measured the levels of TNF-alpha of patients with advanced cirrhosis in monocytes and plasma (Table S2). In patients with advanced cirrhosis (Table S2: patients 1–19), the TNF-alpha mRNA expression of monocytes was significantly

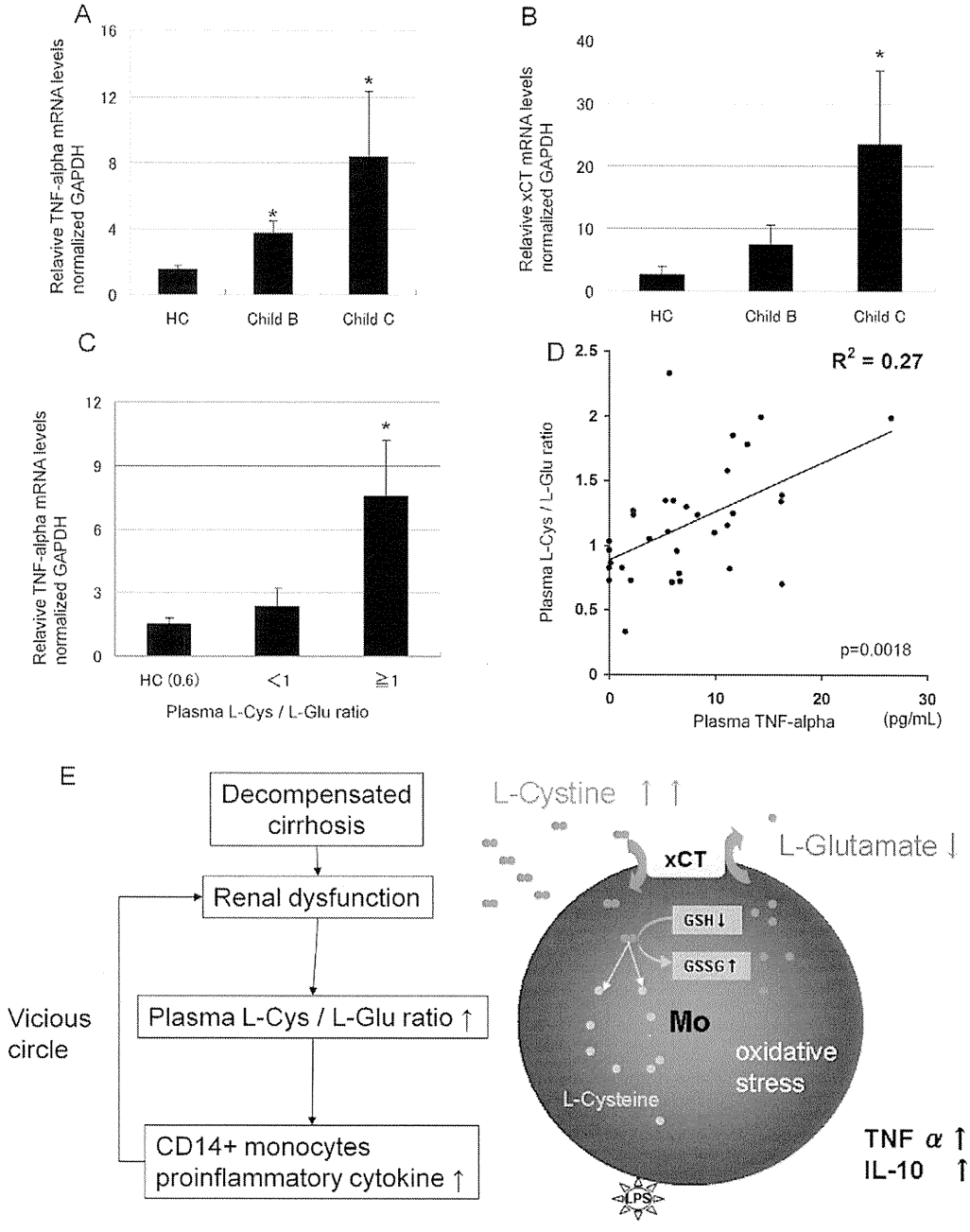

Figure 4. The plasma L-Cys/L-Glu ratio significantly correlated with the plasma TNF-alpha level in patients with advanced cirrhosis. A, CD14+monocytes were isolated from healthy volunteers (n = 5) and patients with adcanced cirrhosis (Table S2 : Patient 1–19). the TNF-alpha relative mRNA levels of CD14+monocytes were determined by real time PCR : delta-delta CT method. All mRNA expression levels were normalized to GAPDH. B, Similarly as in Fig. 4A, the xCT relative mRNA levels of monocytes were determined by real time PCR. C, These patients were separated into a high L-Cys/L-Glu ratio group (≥1) and low ratio group (<1). In healthy control (HC), the average plasma L-Cys/L-Glu ratio was 0.61±0.21. D, Linear regression model was used to model variation in plasma L-Cys/L-Glu ratio and plasma TNF-alpha. R^2 represents coefficient of determination. E, The schematic diagram of the present study concerning monocytes abnormality in patients with decompensated cirrhosis. A,B,C *, $p<0.05$ vs HC (the Mann-Whitney U-test.).
doi:10.1371/journal.pone.0023402.g004

higher than that of healthy controls (Fig. 4A), and xCT mRNA expressions also was increased according to the Child-pugh grade (Fig. 4B). Interestingly, the TNF-alpha mRNA of monocytes was significantly higher in the high plasma L-Cys/L-Glu ratio group (≥ 1) than in the low group (<1) (Fig. 4C). Consistent with these data, the plasma TNF-alpha in the patients was significantly correlated with the plasma L-Cys/L-Glu ratio ($p = 0.0018/r = 0.52247$) (Fig. 4D). We represented the schematic diagram of the present study concerning monocytes abnormality in patients with decompensated cirrhosis (Fig. 4E).

Discussion

Bacterial infections, such as spontaneous bacterial peritonitis (SBP) or pneumonia, are frequent clinical complications and causes of death in patients with advanced cirrhosis [20], because in such immune-compromised patients the innate immune cells can not normally respond to the pathogen [21]. Neutrophils, macrophages, and DCs are important cellular mediators of the innate immune defense. Circulating monocytes, however, are increasingly implicated as essential players in the defense against a range of microbial pathogens [22]. Previously, we made two serum-free media (HCM and ACM) to examine more closely the actual amino acid environment of the living body plasma [9]. First, we showed that plasma L-Cys was increased by renal dysfunction, which is an important factor of the MELD score [18], and showed a significantly positive correlation with the monocyte counts in patient with advanced cirrhosis. However, high levels of L-Cys did not directly influence the proliferation of monocytes in vitro. This paradox raises the possibility that the GM-CSF from PBMCs (Fig. 2E) may indirectly increase the peripheral monocyte counts, because the increase is almost entirely due to the release from bone marrow [23]. This issue should be evaluated in future studies. Second, we showed that extracellular L-Cys dose-dependently increases pro-inflammatory cytokines from monocytes with LPS under the amino acid environment of patients with advanced cirrhosis. Concerning the mechanism that underlies these phenomena, we confirmed that high extracellular levels of L-Cys enhanced the exchange L-Cys/L-Glu antiport of monocytes via xCT, and decreased the intracellular GSH/GSSG ratio under the amino acid condition of advanced cirrhosis. A previous study showed that oxidized Eh L-Cysteine/L-Cys induces the upregulation of nuclear factor-kappa B of monocytes in vitro [24]. These studies support our results. However, the same studies reported that the oxidized extracellular Cys/CySS redox state had no effect on cellular GSH/GSSG redox [24,25]. We think that such differences were probably caused by differences in the culture condition and stimulation period of the immune cells, and that our culture conditions more closely matched the actual amino acid environment of patients with advanced cirrhosis. However, we need to investigate in detail by separate quantification of the reduced form, L-Cysteine; the oxidized form, L-Cys; and the mixed protein L-Cysteine disulfide. Furthermore, we think that a low level of plasma L-Glu enhances the antiport in patients with advanced cirrhosis, because another study reported on a L-Cys transport system whose activity was inhibited by L-Glu in mammalian cultured cells [26].

Finally, we confirmed that the TNF-alpha mRNA of CD14 monocytes, isolated from patients with advanced cirrhosis, was at a higher level than in healthy controls. Furthermore, the value of plasma TNF-alpha showed a significantly positive correlating with the plasma L-Cys/L-Glu ratio.

This present results still cannot be construed as conclusive evidence of a change in the immune system in patients with advanced cirrhosis. We need to investigate whether L-Cys/L-Glu imbalance influences other immune cells such as macrophages, dendritic cells, T-cells and B-cells, and their interaction, and whether the level of L-Glu influences the immune system, because previous studies reported that glutamate is a immunomediator in the intercellular cross-talk between DC and T cells [12,14,27]. In conclusion, we demonstrated for the first time that an L-Cys/L-Glu imbalance, especially high levels of L-Cys, increases pro-inflammatory cytokines, especially TNF-alpha from peripheral CD14+ monocytes under the amino acid condition of advanced cirrhosis in vitro, and these results are consistent with the relationships among plasma L-Cys and TNF-alpha in patients with advanced cirrhosis. This study may provide a new approach for future studies to ameliorate the immune dysfunction in patients with advanced cirrhosis.

Supporting Information

Figure S1 Linear regression model was used to model variation in plasma L-Cys and monocyte count. Among all twenty kinds of free amino acids, only L-Cys was significantly correlated with the monocyte counts in patients with advanced cirrhosis.
(TIF)

Table S1 The serum free culture media used in this study. 'ACM (advanced cirrhotic medium) consistent with the average concentration of plasma amino acids from patients (Child-Pugh grade B or C, n = 90). ACM+Cys: Varying concentrations of L-Cys were added to L-Cys-free ACM, and the final concentration was adjusted to 100–300 nmol/mL. ACM dep Cys: L-Cys free ACM. Other components except amino acids, were identical among media. The amino acid concentrations are expressed in nmol/mL. Fischer's ratio = (Valine+Leucine+Isoleucine)/(Tyrosine+Phenylalanine). We verified that there was no difference between the theoretical value and actual value examined by high performance liquid chromatography.
(DOC)

Table S2 Characteristics of study participants. LC-C: liver cirrhosis due to HCV LC-B: liver cirrhosis due to HBV HCC: hepatocellular carcinoma PBC: Primary biliary cirrhosis Alcoholic: Alcoholic cirrhosis NASH: non alcoholic steatohepatitis HA: Hepatic Encephalopathy PLT: platelet counts ($\times 10^3/\mu L$) PT-INR: prothrombin time-international normalized ratio AST/ALT: aspartate amino transferase/alanine amino transferase (IU/L) Total Bilirubin (mg/dL) Albumin (g/dL) Fischer's ratio mean: L-Valine+L-Leucine+L-Isoleucine/L-Tyrosine+L-Phenylalanine.
(DOC)

Acknowledgments

We thank Dr. Hideyo Sato (University of Yamagata) for thoughtful discussions and Sonoko Ishizaki (Ajinomoto Pharmaceuticals Co) for helpful suggestions. We thank Takeshi Sato (Cell Science & Technology Institute, Inc, Sendai, Japan.) for providing the high quality serum free media. We thank Chikako Sato for excellent technical assistance.

Author Contributions

Conceived and designed the experiments: EK YU YK JI MN KF TS. Performed the experiments: EK YK JI MN OK YW. Analyzed the data: EK YU KF KT TS. Contributed reagents/materials/analysis tools: EK YU YK JI MN. Wrote the paper: EK YU YK TS.

References

1. Tilg H, Wilmer A, Vogel W, Herold M, Nolchen B, et al. (1992) Serum levels of cytokines in chronic liver diseases. Gastroenterology 103: 264–274.
2. Byl B, Roucloux I, Crusiaux A, Dupont E, Deviere J (1993) Tumor necrosis factor alpha and interleukin 6 plasma levels in infected cirrhotic patients. Gastroenterology 104: 1492–1497.
3. Riordan SM, Skinner N, Nagree A, McCallum H, McIver CJ, et al. (2003) Peripheral blood mononuclear cell expression of toll-like receptors and relation to cytokine levels in cirrhosis. Hepatology 37: 1154–1164.
4. Ubeda M, Munoz L, Borrero MJ, Diaz D, Frances R, et al. (2010) Critical role of the liver in the induction of systemic inflammation in rats with preascitic cirrhosis. Hepatology 52: 2086–2095.
5. Navasa M, Follo A, Filella X, Jimenez W, Francitorra A, et al. (1998) Tumor necrosis factor and interleukin-6 in spontaneous bacterial peritonitis in cirrhosis: relationship with the development of renal impairment and mortality. Hepatology 27: 1227–1232.
6. Gines P, Schrier RW (2009) Renal failure in cirrhosis. N Engl J Med 361: 1279–1290.
7. Morgan MY, Marshall AW, Milsom JP, Sherlock S (1982) Plasma amino-acid patterns in liver disease. Gut 23: 362–370.
8. Kakazu E, Kanno N, Ueno Y, Shimosegawa T (2007) Extracellular branched-chain amino acids, especially valine, regulate maturation and function of monocyte-derived dendritic cells. J Immunol 179: 7137–7146.
9. Kakazu E, Ueno Y, Kondo Y, Fukushima K, Shiina M, et al. (2009) Branched chain amino acids enhance the maturation and function of myeloid dendritic cells ex vivo in patients with advanced cirrhosis. Hepatology 50: 1936–1945.
10. Walshe JM, Senior B (1955) Disturbances of cystine metabolism in liver disease. J Clin Invest 34: 302–310.
11. Lemberg A, Fernandez MA (2009) Hepatic encephalopathy, ammonia, glutamate, glutamine and oxidative stress. Ann Hepatol 8: 95–102.
12. Pacheco R, Oliva H, Martinez-Navio JM, Climent N, Ciruela F, et al. (2006) Glutamate released by dendritic cells as a novel modulator of T cell activation. J Immunol 177: 6695–6704.
13. Eck HP, Droge W (1989) Influence of the extracellular glutamate concentration on the intracellular cyst(e)ine concentration in macrophages and on the capacity to release cysteine. Biol Chem Hoppe Seyler 370: 109–113.
14. D'Angelo JA, Dehlink E, Platzer B, Dwyer P, Circu ML, et al. (2010) The cystine/glutamate antiporter regulates dendritic cell differentiation and antigen presentation. J Immunol 185: 3217–3226.
15. Sato H, Shiiya A, Kimata M, Maebara K, Tamba M, et al. (2005) Redox imbalance in cystine/glutamate transporter-deficient mice. J Biol Chem 280: 37423–37429.
16. Sato H, Tamba M, Ishii T, Bannai S (1999) Cloning and expression of a plasma membrane cystine/glutamate exchange transporter composed of two distinct proteins. J Biol Chem 274: 11455–11458.
17. Matsuo S, Imai E, Horio M, Yasuda Y, Tomita K, et al. (2009) Revised equations for estimated GFR from serum creatinine in Japan. Am J Kidney Dis 53: 982–992.
18. Kamath PS, Wiesner RH, Malinchoc M, Kremers W, Therneau TM, et al. (2001) A model to predict survival in patients with end-stage liver disease. Hepatology 33: 464–470.
19. Dennis PB, Jaeschke A, Saitoh M, Fowler B, Kozma SC, et al. (2001) Mammalian TOR: a homeostatic ATP sensor. Science 294: 1102–1105.
20. Gustot T, Durand F, Lebrec D, Vincent JL, Moreau R (2009) Severe sepsis in cirrhosis. Hepatology 50: 2022–2033.
21. Galbois A, Thabut D, Tazi KA, Rudler M, Mohammadi MS, et al. (2009) Ex vivo effects of high-density lipoprotein exposure on the lipopolysaccharide-induced inflammatory response in patients with severe cirrhosis. Hepatology 49: 175–184.
22. Serbina NV, Jia T, Hohl TM, Pamer EG (2008) Monocyte-mediated defense against microbial pathogens. Annu Rev Immunol 26: 421–452.
23. Van Furth R, Diesselhoff-den Dulk MC, Mattie H (1973) Quantitative study on the production and kinetics of mononuclear phagocytes during an acute inflammatory reaction. J Exp Med 138: 1314–1330.
24. Go YM, Jones DP (2005) Intracellular proatherogenic events and cell adhesion modulated by extracellular thiol/disulfide redox state. Circulation 111: 2973–2980.
25. Iyer SS, Accardi CJ, Ziegler TR, Blanco RA, Ritzenthaler JD, et al. (2009) Cysteine redox potential determines pro-inflammatory IL-1beta levels. PLoS One 4: e5017.
26. Bannai S, Kitamura E (1980) Transport interaction of L-cystine and L-glutamate in human diploid fibroblasts in culture. J Biol Chem 255: 2372–2376.
27. Fallarino F, Volpi C, Fazio F, Notartomaso S, Vacca C, et al. (2010) Metabotropic glutamate receptor-4 modulates adaptive immunity and restrains neuroinflammation. Nat Med 16: 897–902.

Am J Physiol Gastrointest Liver Physiol 301: G297–G305, 2011.
First published May 19, 2011; doi:10.1152/ajpgi.00418.2010.

Knockout of the neurokinin-1 receptor reduces cholangiocyte proliferation in bile duct-ligated mice

Shannon Glaser,[1,2,3] Eugenio Gaudio,[5] Anastasia Renzi,[2,5] Romina Mancinelli,[5] Yoshiyuki Ueno,[6] Julie Venter,[2,3] Mellanie White,[2,3] Shelley Kopriva,[2] Valorie Chiasson,[2] Sharon DeMorrow,[2,3] Heather Francis,[2,3,4] Fanyin Meng,[2,4] Marco Marzioni,[7] Antonio Franchitto,[5] Domenico Alvaro,[8] Scott Supowit,[9] Donald J. DiPette,[9] Paolo Onori,[10]* and Gianfranco Alpini[1,2,3]*

[1]*Division of Research, Central Texas Veterans Health Care System,* [2]*Department of Medicine,* [3]*Scott & White Digestive Disease Research Center, and* [4]*Division of Research and Education, Scott & White and Texas A&M Health Science Center College of Medicine, Temple, Texas;* [5]*Department of Anatomical, Histological, Forensic Medicine and Orthopedics Sciences, University of Rome "La Sapienza," Rome, Italy;* [6]*Division of Gastroenterology, Tohoku University Graduate School of Medicine, Aobaku, Sendai, Japan;* [7]*Department of Gastroenterology, Università Politecnica delle Marche, Ospedali Riuniti General Hospital of Ancona, Italy;* [8]*Division of Gastroenterology, Department of Clinical Medicine, Polo Pontino, University of Rome, "Sapienza," Rome, Italy;* [9]*Division of Cell Biology and Anatomy, Medicine, University of South Carolina Medical School, Columbia, South Carolina; and* [10]*Experimental Medicine, University of L'Aquila, L'Aquila, Italy*

Submitted 16 September 2010; accepted in final form 6 May 2011

Glaser S, Gaudio E, Renzi A, Mancinelli R, Ueno Y, Venter J, White M, Kopriva S, Chiasson V, DeMorrow S, Francis H, Meng F, Marzioni M, Franchitto A, Alvaro D, Supowit S, DiPette DJ, Onori P, Alpini G. Knockout of the neurokinin-1 receptor reduces cholangiocyte proliferation in bile duct-ligated mice. *Am J Physiol Gastrointest Liver Physiol* 301: G297–G305, 2011. First published May 19, 2011; doi:10.1152/ajpgi.00418.2010.—In bile duct-ligated (BDL) rats, cholangiocyte proliferation is regulated by neuroendocrine factors such as α-calcitonin gene-related peptide (α-CGRP). There is no evidence that the sensory neuropeptide substance P (SP) regulates cholangiocyte hyperplasia. Wild-type (WT, $^{+/+}$) and NK-1 receptor (NK-1R) knockout (NK-1R$^{-/-}$) mice underwent sham or BDL for 1 wk. Then we evaluated *1*) NK-1R expression, transaminases, and bilirubin serum levels; *2*) necrosis, hepatocyte apoptosis and steatosis, and the number of cholangiocytes positive by CK-19 and terminal deoxynucleotidyl transferase biotin-dUTP nick-end labeling in liver sections; *3*) mRNA expression for collagen 1α and α-smooth muscle (α-SMA) actin in total liver samples; and *4*) PCNA expression and PKA phosphorylation in cholangiocytes. In cholangiocyte lines, we determined the effects of SP on cAMP and D-myo-inositol 1,4,5-trisphosphate levels, proliferation, and PKA phosphorylation. Cholangiocytes express NK-1R with expression being upregulated following BDL. In normal NK-1R$^{-/-}$ mice, there was higher hepatocyte apoptosis and scattered hepatocyte steatosis compared with controls. In NK-1R $^{-/-}$ BDL mice, there was a decrease in serum transaminases and bilirubin levels and the number of CK-19-positive cholangiocytes and enhanced biliary apoptosis compared with controls. In total liver samples, the expression of collagen 1α and α-SMA increased in BDL compared with normal mice and decreased in BDL NK-1R$^{-/-}$ compared with BDL mice. In cholangiocytes from BDL NK-1R $^{-/-}$ mice there was decreased PCNA expression and PKA phosphorylation. In vitro, SP increased cAMP levels, proliferation, and PKA phosphorylation of cholangiocytes. Targeting of NK-1R may be important in the inhibition of biliary hyperplasia in cholangiopathies.

biliary epithelium; cAMP; innervation; mitosis; sensory innervation

HUMAN CHOLANGIOCYTES ARE THE target cells in a number of cholestatic liver diseases (i.e., cholangiopathies) including primary sclerosing cholangitis and primary biliary cirrhosis (5, 28), which are characterized by an abnormal balance between biliary growth and damage (5, 28). In animal models of cholestasis, changes in biliary growth and damage are achieved by a number of pathophysiological maneuvers including extrahepatic bile duct ligation (BDL) (4, 15, 23), acute administration of carbon tetrachloride (CCl_4) (31), cholinergic (30) denervation, and ablation of sensory innervation by knockdown of α-calcitonin gene-related peptide (α-CGRP) (23). In these models, small and large cholangiocytes (lining small and large bile ducts, respectively) (2, 6, 21) show a different biological response, in terms of proliferation, survival, and secretory activity (3, 15, 21, 30, 31). Relevant to this study, in the cholestatic BDL rodent model large but not small cholangiocytes undergo mitosis leading to enhanced large bile duct mass (3, 15, 31). Two second messengers, D-myo-inositol 1,4,5-trisphosphate (IP_3) and cyclic adenosine 3′,5′-monophosphate (cAMP), regulate the proliferative, apoptotic, and secretory functions of small and large cholangiocytes (3, 15–17, 23, 30, 31). Although the IP_3/Ca^{2+}-dependent signaling modulates the function of small cholangiocytes (16, 31), large cholangiocyte hyperplasia following BDL is regulated by the activation of cAMP-dependent PKA signaling (3, 15, 17, 23, 30).

Two afferent nerve pathways are present in the liver: the vagal and the spinal afferent nerve pathways that run through the dorsal root ganglion (45). Sensory nerves also display an efferent function, which is mediated by the release of sensory neuropeptides such α-CGRP from their peripheral terminals in tissues that they innervate modulating cellular functions (25). Substance P (SP), containing peptidergic nerves, is present in the spinal afferent nerve pathway. SP-positive innervation has been localized in the periportal regions of guinea pig and human liver (43). SP is a member of the tachykinin peptide family that is formed by six members: SP, neurokinin A, neurokinin B, neuropeptide K, neuropeptide γ, and hemokinin (1). SP and neurokinin A are present in the central nervous system and primary sensory afferent neurons innervating peripheral tissues and are released from sensory nerve endings both at the level of the spinal cord and in peripheral tissues (1). The tachykinin receptor family consists of three types of seven transmembrane G protein-coupled receptors: neurokinin-1, -2,

* P. Onori and G. Alpini share the last authorship.
Address for reprint requests and other correspondence: G. Alpini, Central Texas Veterans Health Care System and Digestive Disease Research Center and Texas A&M Health Science Center College of Medicine, 702 SW H. K. Dodgen Loop, Temple, TX, 76504 (e-mail: galpini@tamu.edu or galpini@medicine.tamhsc.edu).

and -3 receptors (NK-1R, NK-2R, and NK-3R). SP preferentially binds and signals via the NK-1R (1). Limited data exist regarding the role of sensory innervation in the regulation of biliary functions. Tachykinins are the main nonadrenergic and noncholinergic excitatory neurotransmitters in the common bile duct of guinea pigs (38). Sensory neuropathy has been associated in patients with primary biliary cirrhosis (13). Also, knockout of α-CGRP reduces cholangiocyte hyperplasia in cholestatic BDL mice by downregulation of cAMP signaling (23). No data exist regarding the role of SP in the regulation of biliary hyperplasia during cholestasis induced by BDL.

In many cell types, SP-induced activation of NK-1R (coupled to pertussis toxin-insensitive G_q/G_{11}) activates phospholipase C and subsequent formation of IP_3 and diacylglycerol mobilizing intracellular Ca^{2+} (26, 36). In other cells (27, 37), NK-1R also couple to *1*) $G\alpha_s$ resulting in adenylyl cyclase activation (37) and cAMP formation and *2*) $G\alpha_i$ that inhibits cAMP formation. On the basis of this background, we aim to demonstrate that SP and its receptor, NK-1R, regulate the proliferation of cAMP-dependent large cholangiocytes in the cholestatic BDL mouse model.

MATERIALS AND METHODS

Materials. Reagents were purchased from Sigma Chemical (St. Louis, MO) unless otherwise indicated. The nuclear dye 4,6-diamidino-2-phenylindole (DAPI) was obtained from Molecular Probes, Eugene, OR. The NK-1R antibody against the rat COOH-terminal (393–407) peptide was purchased from Enzo Life Sciences International (Plymouth Meeting, PA). SP was purchased from Phoenix Pharmaceuticals (Burlingame, CA). The antibody against proliferating cell nuclear antigen (PCNA) was purchased from Santa Cruz Biotechnology (Santa Cruz, CA). The mouse anti-cytokeratin-19 (CK-19) antibody (clone RCK105) was purchased from Caltag Laboratories (Burlingame, CA). The cAMP-dependent phospho-PKA catalytic subunit (Thr197) antibody (Cell Signaling, Boston, MA) detects endogenous levels of PKA catalytic subunit (-α, -β, and -γ) only when phosphorylated at Thr197. The cAMP-dependent PKA catalytic subunit-α antibody (Cell Signaling) detects endogenous levels of total PKA catalytic subunit-α. The antibodies for the rabbit anti-ERK1 (which detects p44 and p42) and goat anti-pERK (which detects phosphorylated p44 and p42) were purchased from Santa Cruz Biotechnology RIA kits for the determination of cAMP and IP_3 levels were purchased from GE Healthcare (Arlington Heights, IL).

Animal models. The majority of the studies were performed in wild-type (WT, $^{+/+}$) and NK-1R knockout (NK-1R $^{-/-}$) normal (sham-operated) and 1-wk BDL mice (Table 1); since we did not see

Table 1. *Evaluation of NK-1R expression, liver and body weight, liver-to-body weight ratio in the selected groups of animals*

Groups	NK-1R Expression	Liver Weight, g	Body Weight, g	Liver/body weight × 100, %
WT normal mice (n = 84)	(−/+)	1.98 ± 0.05	26.3 ± 0.5	7.58 ± 0.16
NK-1R$^{-/-}$ normal mice (n = 79)	(−)	1.80 ± 0.05	28.3 ± 0.7	6.25 ± 0.18*
WT BDL mice (n = 41)	(++)	1.94 ± 0.06	21.92 ± 0.3†	8.84 ± 0.21†
NK-1R$^{-/-}$ BDL mice (n = 25)	(−)	2.07 ± 0.09	25.9 ± 0.7‡	7.96 ± 0.27‡

Data are means ± SE. ND, not detectable; NK-1R, neurokinin-1 receptor. *, †$P < 0.05$ vs. the corresponding value of normal wild-type (WT) mice. ‡$P < 0.05$ vs. the corresponding value of WT bile duct-ligated (BDL) mice.

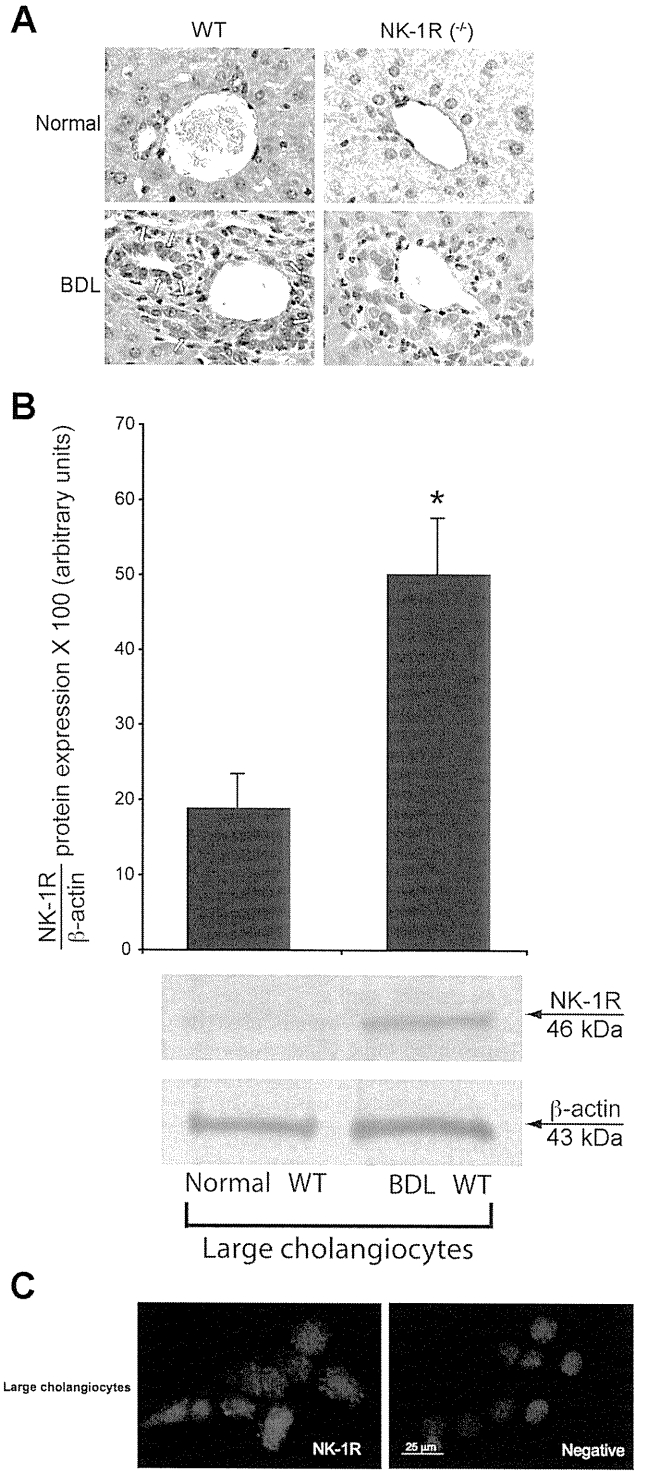

Fig. 1. *A*: expression of NK-1 receptor (NK-1R) was low in bile ducts from normal wild-type (WT; red arrow) mice but increased in bile ducts from bile duct-ligated (BDL) WT mice (yellow arrows; see Table 1). NK-1R was absent in intrahepatic bile ducts from normal and BDL NK-1R knockout (NK-1R$^{-/-}$) mice. Original magnification ×40. *B*: protein expression of NK-1R increased in large cholangiocytes from BDL WT mice compared with large cholangiocytes from normal WT mice. Data are means ± SE of 6 immunoblots derived from protein obtained from cumulative preparations of cholangiocytes. *$P < 0.05$ vs. the corresponding value of BDL large cholangiocytes. *C*: specific immunoreactivity for NK-1R in representative fields of large cholangiocytes is shown in red; cell nuclei were stained with 4,6-diamidino-2-phenylindole (DAPI; blue). Bar size = 25 μm.

Table 2. *Evaluation of serum levels of transaminases and bilirubin*

Groups	Alanine Aminotransferase, units/l	Aspartate Aminotransferase, units/l	Total Bilirubin, mg/l
WT normal mice	20.2 ± 2.4 (n = 8)	55.2 ± 3.9 (n = 8)	<0.1 (n = 8)
NK-1R$^{-/-}$ normal mice	123.8 ± 20.7 (n = 11)	229.3 ± 23.2 (n = 12)	<0.1 (n = 16)
WT BDL mice	687.1 ± 119.1* (n = 6)	1,134.6 ± 212.1* (n = 5)	13.58 ± 1.74* (n = 7)
NK-1R$^{-/-}$ BDL mice	389 ± 35† (n = 6)	708.6 ± 50.6† (n = 5)	9.22 ± 1.1† (n = 7)

Data are means ± SE of 7 evaluations. *P < 0.05 vs. the corresponding value of normal WT mice. †P < 0.05 vs. the corresponding value of WT mice with BDL for 7 days.

any difference in biliary growth between normal and sham-operated mice (not shown), we used normal mice in our studies. Some of the experiments were also performed in normal and 1-wk BDL heterozygous mice (derived from the same breeding) to evaluate hepatocyte apoptosis and steatosis, lobular necrosis, the degree of inflammation and intrahepatic bile duct mass, and biliary apoptosis in vivo. BDL was performed as described (22, 23, 35). The NK-1R$^{-/-}$ mouse model (25–30 g, of the N5 generation) is bred at our Animal Facility; the original breeding pair was a gift from Dr. Norma Gerard (Harvard Medical School, Boston, MA) to Dr. Donald DiPette (coauthor in this article). This is a homozygous$^{-/-}$ model on a C57BL/6 background. The mouse model lacking the NK-1R gene was generated as described (12). Age-matched male C57BL/6 wild-type (WT) mice were purchased from Charles River (Wilmington, MA), whereas heterozygous mice were obtained from our breeding colony. All mice were maintained in a temperature-controlled environment (20–22°C) with 12:12-h light-dark cycles. Before each experimental procedure, animals were injected with pentobarbital sodium (50 mg/kg body wt ip). All animal experiments were performed according to a protocol approved by the Scott and White and Texas A&M Health Science Center Institutional Animal Care and Use Committee.

Immortalized and freshly isolated large cholangiocytes. Since BDL induces the proliferation of large but not small cholangiocytes (21, 23), the signaling studies were performed in freshly isolated large cholangiocytes from WT and NK-1R$^{-/-}$ BDL mice, and our immortalized line of large cholangiocytes, which display phenotypical and functional characteristics similar to those of freshly isolated large cholangiocytes (16, 21, 22). Virtually pure (by CK-19 immunohistochemistry) (16) isolated large cholangiocytes were obtained by centrifugal elutriation followed by immunoaffinity separation (16, 21) by using a monoclonal antibody, mouse IgG2a (provided by Dr. R. Faris, Providence, RI) against an antigen expressed by all intrahepatic cholangiocytes (21).

Evaluation of NK-1R protein expression. Analysis of NK-1R expression was evaluated by semiquantitative immunohistochemistry in paraffin-embedded liver sections (4–5 μm; 6 slides per treatment group; for each slide 6 nonoverlapping fields were evaluated) (16, 21) from the selected groups of animals. Following immunohistochemistry, photographs of liver sections were taken by Leica Microsystems DM 4500 B Light Microscopy (Weltzlar, Germany) with a Jenoptik Prog Res C10 Plus Videocam (Jena, Germany). The quantitative expression of NK-1R was measured by immunoblots (16) in protein (10 μg) from whole cell lysate from large cholangiocytes from normal and BDL WT mice. The intensity of the bands was determined by scanning video densitometry using the phospho-imager Storm 860 and the ImageQuant TL software version 2003.02 (GE Healthcare, Little Chalfont, Buckinghamshire, UK). The presence of NK-1R was also evaluated by immunofluorescence (14, 16) in immortalized large cholangiocytes. Images were visualized via an Olympus IX-71 confocal microscope. For all immunoreactions, negative controls (with normal serum from the same species substituted for the primary antibody) were included.

Evaluation of serum levels of transaminases and bilirubin, lobular necrosis, inflammation, hepatocyte apoptosis and steatosis, and cholangiocyte proliferation and apoptosis. In the in vivo studies, we measured *1*) liver weight, body weight, and liver-to-body weight ratio (4) and *2*) serum levels of transaminases, alanine aminotransferase and aspartate aminotransferase, and total bilirubin using a Dimension RxL Max Integrated Chemistry system (Dade Behring, Deerfield IL) by the Chemistry Department, Scott & White.

We evaluated *1*) lobular necrosis and the degree of inflammation by hematoxylin and eosin (H&E) staining; *2*) the percentage of apoptotic hepatocytes by terminal deoxynucleotidyl transferase biotin-dUTP nick-end labeling (TUNEL) kit (33) (Apoptag; Chemicon International); and *3*) the number of large cholangiocytes (lining large bile ducts, > 15 μm diameter) (2) positive for PCNA (15) and CK-19 (39) or by TUNEL kit (33) in liver sections (4–5 μm; 6 slides per treatment group; for each slide 6 nonoverlapping fields were evaluated) from the selected groups of animals. The degree of hepatocyte steatosis was evaluated in frozen liver sections (4–5 μm thick) by both H&E staining and the oil red O staining kit (32) (IHC World, Woodstock, MD). All sections were examined in a coded fashion by two board certified pathologists by a BX-51 light microscope (Olympus, Tokyo, Japan) equipped with a camera. We also evaluated the damage of a number of tissues/organs in the experimental groups listed in Table 1.

Evaluation of gene expression for collagen 1α and α-smooth muscle actin in total liver samples. We measured the expression of the messages for collagen 1α and α-smooth muscle actin (α-SMA) in RNA (0.5 μg) in total liver tissue by the RT^2 Real-Time assay from SABiosciences (Frederick, MD) (16). A $\triangle\triangle C_T$ (delta delta of the threshold cycle) analysis was performed by using RNA from normal WT mice as the control sample. Data were expressed as relative mRNA levels ± SE of the selected gene-to-GAPDH ratio. The primers for collagen 1α and α-SMA (purchased from SABiosciences) were designed according to the NCBI GenBank Accession numbers: NM_007742 (for collagen 1α) (18) and NM_007392 (for α-SMA) (34).

Measurement of PCNA protein expression and phosphorylation of PKA in purified large cholangiocytes. In protein (10 μg) from whole cell lysate from spleen (positive control) and purified large cholangiocytes from WT and NK-1R$^{-/-}$ BDL mice, we evaluated by immunoblots (16, 21) cholangiocyte proliferation by PCNA protein expression (measured as ratio to β-actin protein expression) (16), and the phosphorylation of cAMP-dependent PKA (expressed as ratio to protein expression of the corresponding total protein), a molecule playing an important role in cAMP-dependent regulation of large cholangiocyte proliferation (8, 15, 17). The intensity of the bands was determined by scanning video densitometry using the phospho-imager

Table 3. *Evaluation of the percentage of hepatocytes positive by TUNEL*

Groups	Percentage of Hepatocytes Positive by TUNEL
WT normal mice	4.2 ± 0.44
NK-1R$^{-/-}$ normal mice	4.9 ± 0.48*
WT 7 BDL mice	31.8 ± 2.3*
NK-1R$^{-/-}$ BDL mice	34.0 ± 2.6

Data are means ± SE. TUNEL, terminal deoxynucleotidyltransferase biotin-dUTP nick-end labeling. *P < 0.05 vs. the corresponding value of normal WT mice.

Storm 860 and the ImageQuant TL software version 2003.02 (GE Healthcare).

In vitro effect of SP on cAMP and IP_3 levels, proliferation, and phosphorylation of PKA and ERK1/2 of immortalized large cholangiocytes. For the measurement of cAMP or IP_3 levels, large immortalized cholangiocytes were treated at room temperature for 5 (cAMP) (3, 15) or 10 (IP_3) (16) min with 0.2% bovine serum albumin (BSA) or SP (10^{-9} M) before evaluation of the levels of these two molecules by RIA (2, 3, 15, 16). In other experiments, large cholangiocyte lines were treated at 37°C for 24, 48, and 72 h with 0.2% BSA or SP (10^{-6} to 10^{-11} M) before evaluation of cell proliferation by CellTiter 96 Cell Proliferation Assay (Promega, Madison, WI) (16). In separate sets of experiments, large cholangiocytes were treated at 37°C for 48 h with 0.2% BSA (basal) or SP (10^{-9} M) for 48 h in the absence or presence of preincubation with spantide (a specific NK-1R inhibitor, 10^{-6} M) (24), BAPTA/AM (5 μM) (16), or H89 (a PKA inhibitor, 30 μM) (22) before evaluation of proliferation by CellTiter 96 Cell Proliferation Assay. Absorbance was measured at 490 nm on a microplate spectrophotometer (Molecular Devices, Sunnyvale, CA). Data were expressed as the fold change of treated cells compared with BSA-treated cells. Also, large cholangiocytes were stimulated with 0.2% BSA or SP (10^{-9} M for 1, 2, and 6 h) before evaluation by immunoblots (19) of the proliferation (by PCNA) and the phosphorylation of PKA. The intensity of the bands was determined by scanning video densitometry (see above). Large cholangiocytes were also stimulated with 0.2% BSA or SP (10^{-9} M for 1, 2, 3, 5, 7, 10, 20, 30, 60, and 90 min, 1, 2, and 6 h) before evaluation of ERK1/2 phosphorylation by immunoblots (19).

Statistical analysis. All data are expressed as means ± SE. Differences between groups were analyzed by the Student's unpaired *t*-test when two groups were analyzed and by ANOVA when more than two groups were analyzed, followed by an appropriate post hoc test.

RESULTS

Expression of NK-1R in liver sections and isolated and immortalized large cholangiocytes. By semiquantitative immunohistochemistry, the expression of NK-1R was low in bile ducts from WT (red arrow) normal mice but increased in bile ducts from WT BDL mice (Fig. 1*A*; yellow arrows and Table 1). NK-1R was absent in bile ducts from normal and BDL NK-$1R^{-/-}$ mice (Fig. 1*A* and Table 1). These findings were confirmed by immunoblotting: the expression of NK-1R increased in large cholangiocytes from BDL WT mice compared with large cholangiocytes from normal WT mice (Fig. 1*B*); NK-1R was also expressed by small bile ducts in liver sections (not shown). By immunofluorescence, specific immunoreactivity for NK-1R in representative fields of large murine cholangiocyte lines (44) is shown in red; cell nuclei were stained with DAPI (blue) (Figs. 1*C*).

Evaluation of serum levels of transaminases and bilirubin, lobular necrosis, inflammation, hepatocyte apoptosis and steatosis, and cholangiocyte proliferation and apoptosis. Surprisingly, body weight was significantly lower in WT BDL mice compared with NK-$1R^{-/-}$ BDL mice (Table 1). In both normal and BDL NK-$1R^{-/-}$ mice there was a significant decrease in liver-to-body weight ratio (an index of liver growth including cholangiocytes) (4) compared with the corresponding WT mice

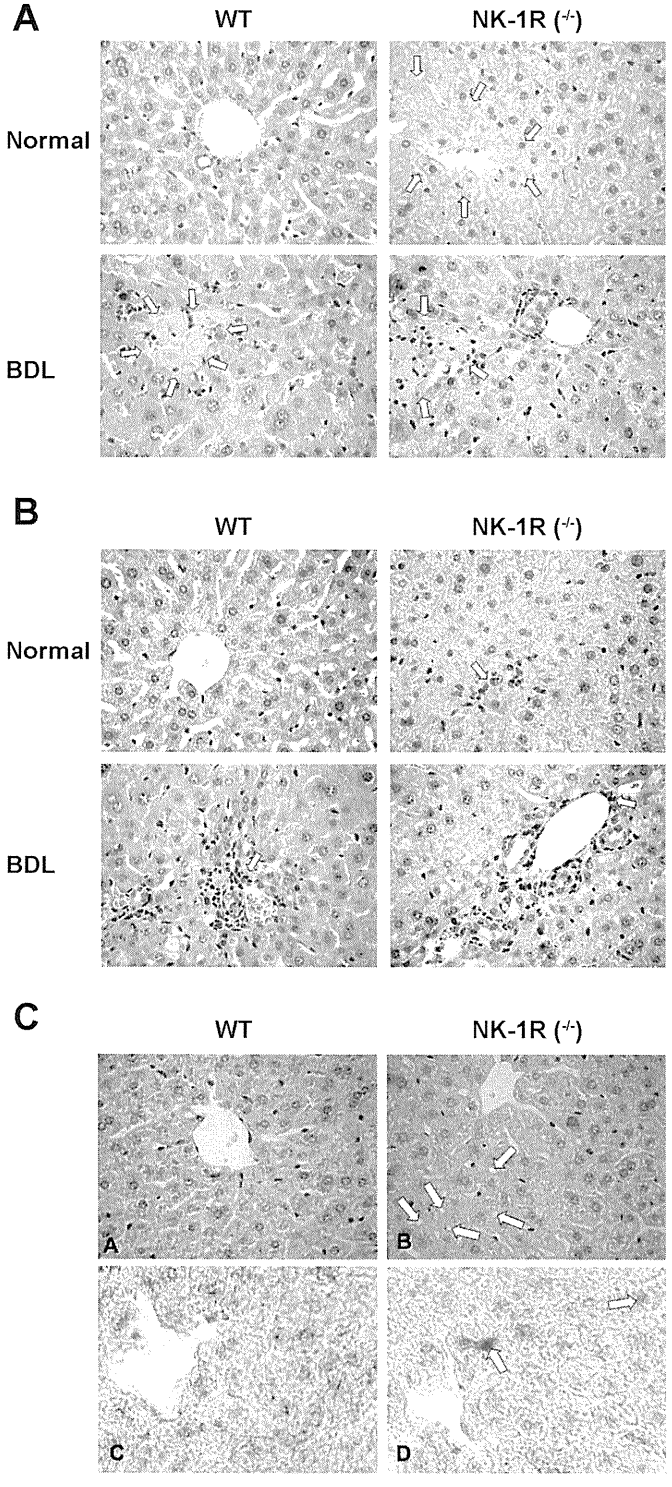

Fig. 2. Evaluation of necrosis (*A*), inflammatory infiltrates (by H&E staining) (*B*), and steatosis [by H&E staining (*CA* and *CB*) and oil red O staining (*CC* and *CD*)] in liver sections from the experimental groups of Table 1. In sections from normal NK-$1R^{-/-}$ mice, we observed some necrotic areas (yellow arrows; *A*) and inflammatory infiltrates (yellow arrow *B*) compared with normal WT mice. There was a decrease in necrotic areas in NK-$1R^{-/-}$ BDL mice compared with BDL WT mice. No marked difference in inflammatory infiltrate was observed between WT and NK-$1R^{-/-}$ BDL mice. By hematoxylin and eosin (H&E; *CA* and *CB*) and oil red O (*CC* and *CD*) staining, in NK-$1R^{-/-}$ normal mice, centrolobular liver parenchyma shows round-shaped areas (yellow arrows) evocative of steatosis (*CB*) and scattered red areas highlighted by oil red O stain method, a specific stain for neutral lipids (yellow arrows) (*CD*). WT normal mice samples show normal liver morphology without oil red O stain (*CA* and *CC*). (Light microscopy: *CA* and *CB*, H&E, original magnification ×20; *CC* and *CD*, oil red O staining in frozen liver sections, original magnification ×40).

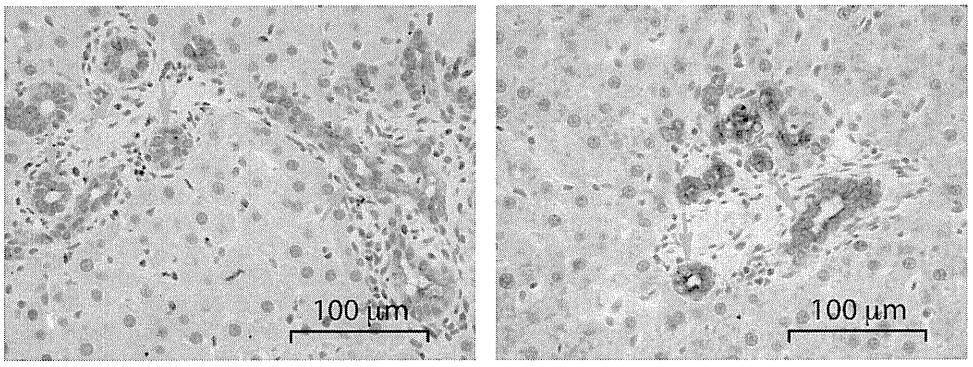

Fig. 3. Immunohistochemistry for CK-19 in liver sections from WT and NK-1R$^{-/-}$ BDL mice. There was a decrease in the number of large CK-19-positive cholangiocytes in liver sections from NK-1R$^{-/-}$ BDL mice compared with 7-day BDL WT mice (for semiquantitative data, see Table 4). Original magnification ×40.

(Table 1). In agreement with previous studies in rodents (4), the serum levels of transaminases (alanine aminotransferase and aspartate aminotransferase) and total bilirubin were higher in WT BDL mice compared with normal WT mice and decreased in NK-1R$^{-/-}$ BDL mice compared with WT BDL mice (Table 2). No difference in the serum levels of total bilirubin was observed between WT normal mice and NK-1R$^{-/-}$ normal mice (Table 2). Surprisingly, we observed a significant increase in the serum levels of transaminases in normal NK-1R$^{-/-}$ mice compared with WT normal mice (Table 2).

In liver sections from normal NK-1R$^{-/-}$ mice, we observe higher hepatocyte apoptosis (Table 3), some necrotic areas (yellow arrows, Fig. 2*A*) and inflammatory infiltrates (yellow arrow, Fig. 2*B*) compared with normal WT mice. There was a decrease in necrotic areas in NK-1R$^{-/-}$ BDL mice compared with BDL WT mice (see yellow arrows) (Fig. 2*A*). No marked difference in inflammatory infiltrate was observed between WT and NK-1R$^{-/-}$ BDL mice (see yellow arrow) (Fig. 2*B*). In NK-1R$^{-/-}$ normal mice, centrolobular liver parenchyma shows round-shaped areas (Fig. 2*C*) and red scattered spots by oil red O staining evocative of steatosis (Fig. 2*C*), whereas WT (Fig. 2*C*) and heterozygous (not shown) normal mice samples display normal liver morphology. All BDL liver sections do not present round-shaped areas evocative of steatosis (not shown). No significant differences in these parameters were seen between WT and NK-1R$^{-/-}$ normal mice (not shown). These histomorphological changes (Fig. 2, *A–C* and Table 3) likely explain the significant increase in the serum levels of transaminases observed in normal NK-1R$^{-/-}$ mice compared with WT normal mice. The number of PCNA-positive cholangiocytes was low and similar in both WT (0.4 ± 0.2) and NK-1R$^{-/-}$ (0.2 ± 0.2) normal mice. In NK-1R$^{-/-}$ BDL mice, there was a decrease in the number of PCNA-positive large cholangiocytes (17.4 ± 1.3) compared with WT BDL mice (12.0 ± 1.3). The number of CK-19-positive large cholangiocytes was similar among WT, heterozygous, and NK-1R$^{-/-}$ normal mice and increased following BDL in both WT and heterozygous BDL mice (Fig. 3 and Table 4). In NK-1R$^{-/-}$ BDL mice, there was a decrease in the number of CK-19-positive large cholangiocytes compared with WT BDL mice (Fig. 3 and Table 4). In heterozygous BDL mice, the number of CK-19-positive cholangiocytes was lower than that of BDL WT mice but higher than NK-1R$^{-/-}$ BDL mice (Table 4). In NK-1R$^{-/-}$ and heterozygous BDL mice, there was a concomitant increase in the number of TUNEL-positive large cholangiocytes compared with the degree of cholangiocyte apoptosis observed in the corresponding WT BDL mice (Table 4). No difference in cholangiocyte apoptosis was observed between WT and heterozygous normal mice and NK-1R$^{-/-}$ normal mice (Table 4). No significant gross postmortem or pathological changes were detected in the body cavities, integumentary, alimentary, respiratory, circulatory, nervous, urogenital, hematopoietic, and musculoskeletal systems of normal WT mice and NK-1R$^{-/-}$ normal mice (not shown).

mRNA expression for collagen 1α and α-SMA. No changes in the mRNA and protein expression of collagen 1α were observed in total liver samples from WT and NK-1R$^{-/-}$ normal mice (Fig. 4*A*). The expression of α-SMA decreased in total liver samples from normal NK-1R$^{-/-}$ mice compared with normal WT mice (Fig. 4*B*). The expression of collagen 1α and α-SMA increased in total liver samples from BDL WT mice compared with normal WT mice (Fig. 4, *A* and *B*). There was a decrease expression of collagen 1α and α-SMA mRNA expression in total liver samples from BDL NK-1R$^{-/-}$ mice compared with total liver samples from BDL WT mice (Fig. 4, *A* and *B*).

Measurement of PCNA protein expression, and phosphorylation of cAMP-dependent PKA in isolated large cholangiocytes. There was a decrease in PCNA expression in large cholangiocytes from NK-1R$^{-/-}$ BDL mice compared with large cholangiocytes from WT BDL mice (Fig. 5*A*). In large cholangiocytes from NK-1R$^{-/-}$ BDL mice there was a decrease in the phosphorylation of cAMP-dependent PKA compared with large cholangiocytes from WT BDL mice (Fig. 5*B*).

Table 4. *Evaluation of the number of CK-19 or TUNEL-positive large cholangiocytes*

Groups	Number of CK-19-Positive Cholangiocytes	Number of Cholangiocytes Positive by TUNEL
WT normal mice	17.2 ± 1.0	ND
Heterozygous normal mice	17.3 ± 1.1	ND
NK-1R$^{-/-}$ normal mice	17.1 ± 1.8	0.3 ± 0.1
WT 7 BDL mice	78.8 ± 4.3*	1.2 ± 0.2
Heterozygous BDL mice	65.1 ± 2.0*	4.2 ± 0.2
NK-1R$^{-/-}$ BDL mice	53.0 ± 2.6†	6.6 ± 0.4†

Data are means ± SE. *$P < 0.05$ vs. the corresponding value of normal WT mice. †$P < 0.05$ vs. the corresponding value of WT mice with BDL for 7 days.

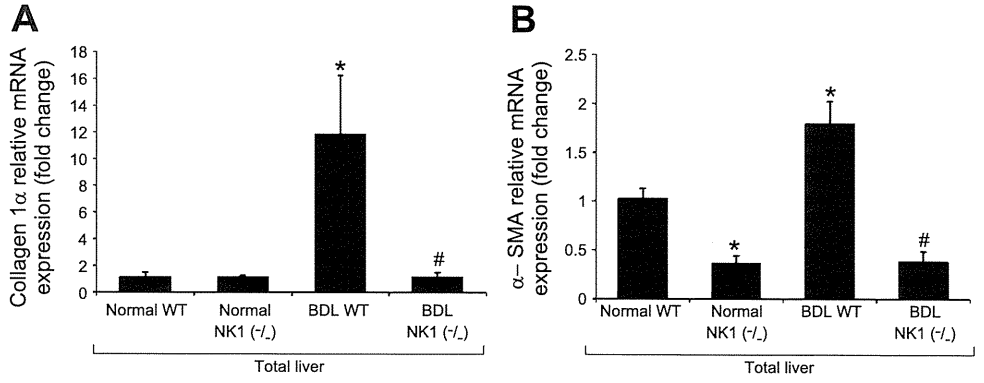

Fig. 4. Evaluation of the mRNA and protein expression of collagen 1α (*A*) and α-smooth muscle actin (α-SMA; *B*) in total liver tissue from WT and NK-1R$^{-/-}$ normal and BDL mice. No changes in the expression of collagen 1α were observed in total liver samples from normal WT and normal NK-1R$^{-/-}$ mice. The expression of α-SMA decreased in total liver samples from normal NK-1R$^{-/-}$ mice compared with normal WT mice. The expression of collagen 1α and α-SMA increased in total liver samples from BDL WT mice compared with normal WT mice. There was a decrease expression of collagen 1α and α-SMA mRNA expression in total liver samples from BDL NK-1R$^{-/-}$ mice compared with total liver samples from BDL WT mice. *$P < 0.05$ vs. the corresponding value of normal WT mice. #$P < 0.05$ vs. the corresponding value of WT BDL mice.

In vitro effect of SP on cAMP and IP_3 levels, cholangiocyte proliferation, and phosphorylation of PKA and ERK1/2 of large cholangiocytes. A marked increase in cAMP levels was observed with forskolin (an activator of adenylyl cyclase) (17), whereas secretin and SP induced a modest yet significant increase in cAMP levels in large cholangiocytes (Fig. 6*A*). The increase in cAMP levels observed with secretin in immortalized large cholangiocytes was similar to that observed in our previous studies (17). SP did not increase IP_3 levels of large cholangiocytes (Fig. 6*B*). By MTS assays, SP induced a similar and sustained (both at 48 and 72 h) increases in the proliferation of large cholangiocytes compared with controls (Fig. 7, *A* and *B*); no increase was seen at 24 h of treatment with SP (not shown). SP stimulation of large cholangiocyte growth was blocked by preincubation with spantide and H89 at 48 h and partly at 72 h (Fig. 7 *C* and *D*); BAPTA/AM did not block substance stimulation of large cholangiocyte proliferation (Fig. 7 *C* and *D*). Short-term treatment with SP increased PCNA protein expression and phosphorylation of PKA (but not ERK1/2, not shown) compared with controls (Fig. 8, *A* and *B*).

DISCUSSION

Previous studies have demonstrated that *1*) circulating levels of the sensory neuropeptides CGRP, SP, and adrenomedullin are elevated in humans, and rodent models of cirrhosis and biliary hyperplasia (11, 23, 29, 40); and *2*) SP serum levels are elevated in cholestatic patients and BDL rats (42). Our study provides the first evidence regarding the role of the SP→NK-1R axis in sustaining the proliferation of large cholangiocytes by activation of cAMP signaling. We found an increase in the serum levels of transaminases in normal NK-1R$^{-/-}$ mice compared with WT normal mice. The serum levels of transaminases and total bilirubin were decreased in NK-1R$^{-/-}$ BDL mice compared with WT BDL mice. We demonstrated the presence of NK-1R in large cholangiocytes that was higher in BDL compared with normal rats. Knockdown of the NK-1R gene in BDL mice induces a decrease (~40%) in the number of large cholangiocytes (associated with enhanced biliary apoptosis) compared with BDL WT mice. There was decreased PCNA protein expression and phosphorylation of PKA in large cholangiocytes from NK-1R$^{-/-}$ BDL mice

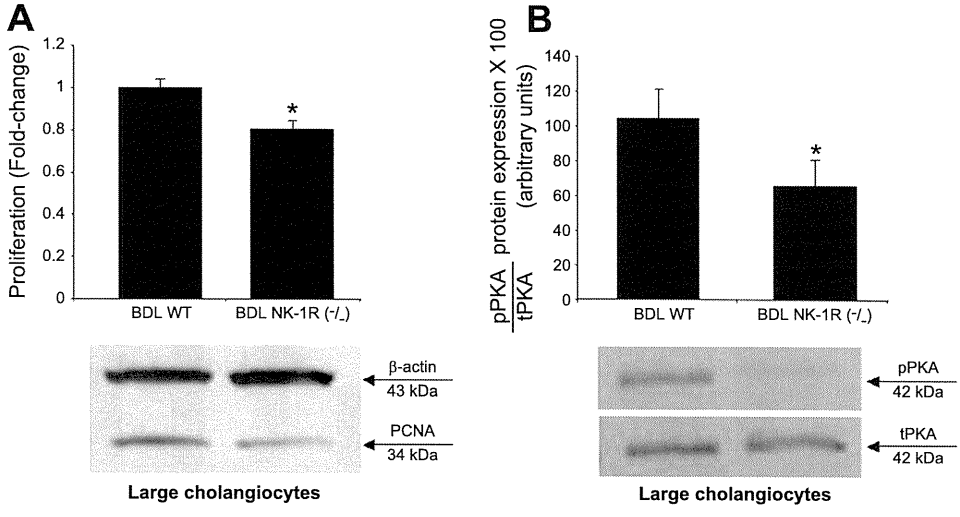

Fig. 5. Evaluation of PCNA expression and cAMP-dependent phosphorylation of PKA in large cholangiocytes from WT and NK-1R$^{-/-}$ BDL mice. There was decreased PCNA expression (*A*) and phosphorylation of PKA (*B*) in large cholangiocytes from NK-1R$^{-/-}$ BDL mice compared with large cholangiocytes from WT BDL mice. Data are means ± SE of 6 immunoblots derived from protein obtained from cumulative preparations of cholangiocytes. pPKA, phosphorylated PKA; tPKA, total PKA. *$P < 0.05$ vs. the corresponding value of BDL large cholangiocytes. *$P < 0.05$ vs. the corresponding value of BDL large cholangiocytes.

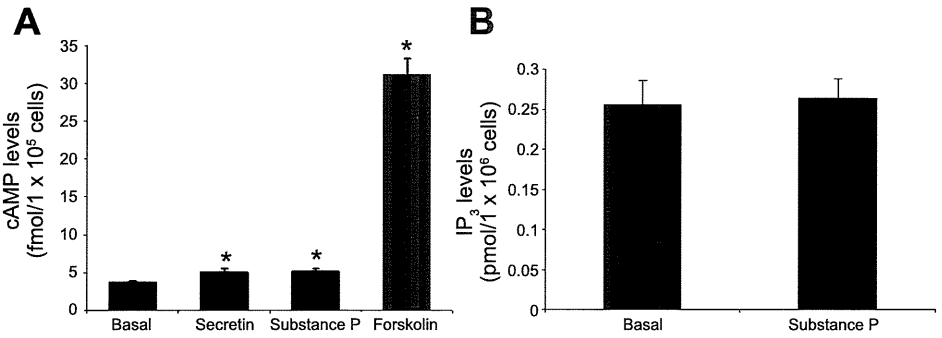

Fig. 6. In vitro effect of forskolin (10^{-4} M), secretin (100 nM) and substance P (10 μM) on cAMP (*A*) and substance P (10 μM) on D-myo-inositol 1,4,5-trisphosphate (IP_3) levels (*B*) of large cholangiocytes. *A*: a massive increase in cAMP levels was observed with forskolin, whereas secretin and substance P induced a modest albeit significant increase in cAMP levels in large cholangiocytes. *B*: substance P did not increase IP_3 levels of large cholangiocytes. Substance P increased cAMP (*A*) but not IP_3 (*B*) levels of large cholangiocytes. Data are means ± SE of 6 values obtained from cumulative preparations of cholangiocytes. *$P < 0.05$ vs. the corresponding basal value of large cholangiocytes treated with 0.2% BSA (basal).

compared with controls. The expression of collagen 1α and α-SMA increased in total liver samples from BDL WT mice compared with normal WT mice and decreased in BDL NK-$1R^{-/-}$ mice compared with total liver samples from BDL WT mice. In vitro, SP increased cAMP levels, enhanced the phosphorylation of PKA but not ERK1/2, and induced a sustained increase in the proliferation of large cholangiocytes. Pharmacological targeting of NK-1R may be important in the inhibition of biliary proliferation in cholestatic liver disorders.

In support for the presence of NK-1R in liver, previous studies have demonstrated the presence of NK-1R in hepatocytes (9, 10). Although both small (not shown) and large cholangiocytes express NK-1R, we evaluated the role of the SP→NK-1R axis on the regulation of large cholangiocyte growth since large, but not small, cholangiocytes proliferate in response to BDL (3, 15, 31). Previous studies have emphasized the importance of cAMP/PKA/ERK1/2 signaling in the regulation of large biliary functions (8). For example, the stimulation of adenylyl cyclase by forskolin stimulates large cholangiocyte proliferation (17). Maintenance of cholangiocyte cAMP levels by administration of forskolin prevents the functional damage of bile ducts induced by vagotomy (30). Since *1*) small cholangiocytes (whose function is regulated by IP_3/Ca^{2+}) (16, 20) express NK-1R and *2*) SP exerts its cellular function by the activation of both cAMP and IP_3/Ca^{2+} signaling (26, 36), studies aimed to evaluate the role of SR in small cholangiocyte functions are necessary. Also, further experiments aimed to evaluate the effects of SP on the phosphorylation of other MAPK isoforms such as JNK and p38 in large cholangiocytes are underway and part of another project.

In our NK-$1R^{-/-}$ BDL model, the extent of the reduction (~40%) of biliary mass is consistent with the concept that cholangiocyte proliferation is coordinately modulated by a number of stimulatory/inhibitory neuroendocrine factors (7). A similar reduction in biliary was observed in α-CGRP $BDL^{-/-}$ mice (23) since other sensory neuropeptides such as β-CGRP

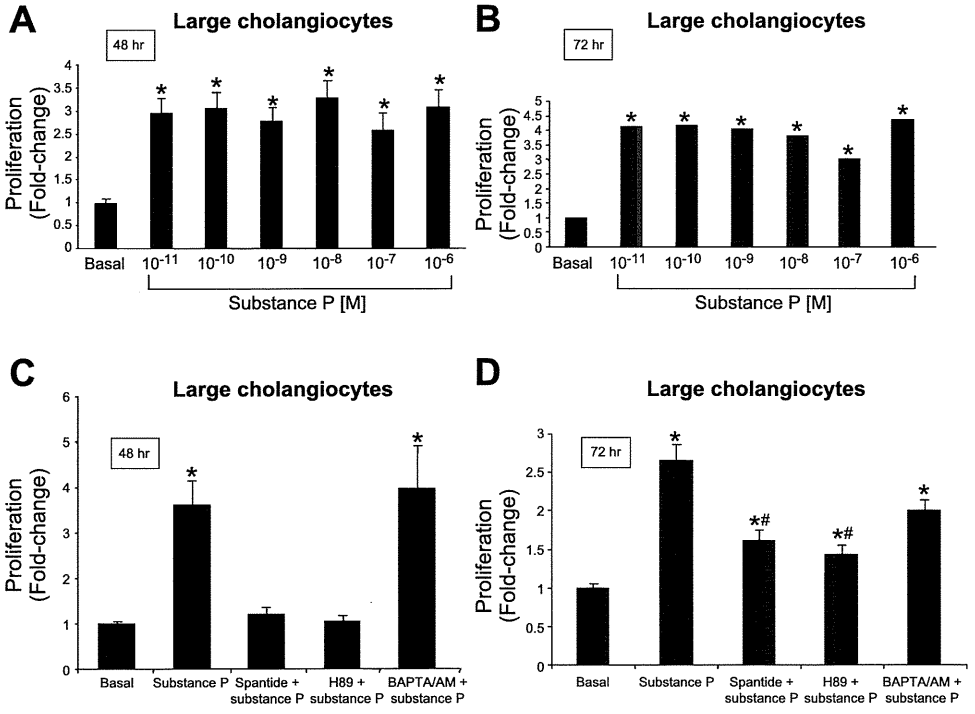

Fig. 7. *A* and *B*: by MTS assays, substance P induced a similar (at all the doses used) and sustained (24 and 72 h) increase in the proliferation of large cholangiocytes compared with BSA-treated cells. Data are means ± SE of 6 experiments. *$P < 0.05$ vs. the corresponding basal value of large cholangiocytes. *C* and *D*: effect of 0.2% BSA (basal) or substance P (10^{-9} M) for 48 h in the absence or presence of preincubation with spantide (specific NK-1R inhibitor), H89 (PKA inhibitor), or BAPTA/AM (intracellular Ca^{2+} chelator). Substance P stimulation of large cholangiocyte growth was blocked by preincubation with spantide and H89 but not BAPTA/AM. Data are means ± SE of 6 experiments. *$P < 0.05$ vs. the corresponding basal value of large cholangiocytes.

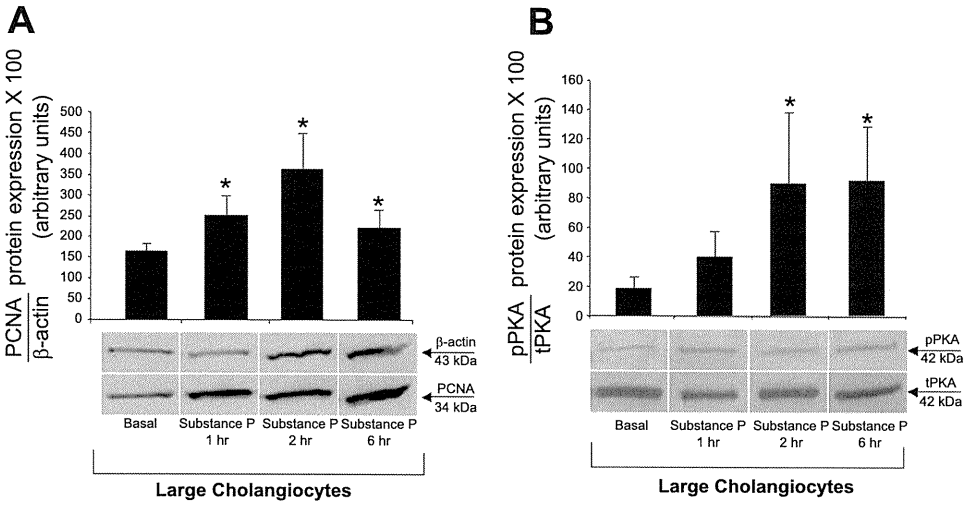

Fig. 8. Effect of 0.2% BSA (basal) or substance P (10^{-9} M for 1, 2, and 6 h) on the proliferation (by PCNA) and phosphorylation of PKA of large cholangiocytes. Substance P increased PCNA protein expression (*A*) and the phosphorylation of PKA (*B*) compared with their corresponding basal values. Data are means ± SE of 10 immunoblots for PCNA (*A*) and 7 immunoblots for PKA derived from protein (10 μg) (*B*) obtained from cumulative preparations of cholangiocytes. *$P < 0.05$ vs. the corresponding value of large cholangiocytes treated with BSA.

stimulate cholangiocyte proliferation during cholestasis. Also, knockout of the secretin receptor gene induces a similar decrease in biliary mass in mice with BDL (22). The reduction of the serum levels of transaminases and bilirubin observed in NK-1R$^{-/-}$ BDL mice further supports the concept that blockage of the NK-1R induced signaling is important in the reduction of liver damage and biliary hyperplasia. The increase in hepatocyte apoptosis and steatosis likely explains the significant increase in the serum levels of transaminases observed in normal NK-1R$^{-/-}$ mice compared with WT normal mice. This finding also suggests that SP signaling may play a role in hepatic metabolism and that lack of the NK-1R may trigger hepatocyte steatosis (41) that was we speculate was resolved during cholestasis induced by BDL. Compared with WT animals, in NK-1R$^{-/-}$ mice a significant reduction in the mRNA expression of collagen 1α and α-SMA after BDL. These data reflect the reduction of the expansion of the biliary tree in NK-1R$^{-/-}$ mice, with a consequent reduction of biliary fibrogenesis, which is mostly likely due to reduced hepatic stellate cell activity (46). In addition to alterations in hepatic stellate cell activation, we cannot rule out that an ancillary part of those differences may be accounted to reduced collagen deposition by hepatocytes, by cholangiocytes, and, in particular, by inflammatory cells, since SP is a one of the mediators of neurogenic inflammation and NK1-R antagonist have been shown to protect mice from cytokine, CD95 and TNF-α mediated liver injury (9, 10).

The biological and pathophysiological significance of our findings is supported by a number of studies. For example, the neurokinin-1 receptor antagonists CP-96,345 and L-733,060 protect mice from cytokine-mediated liver injury, most likely by inhibiting SP effects (10). NK-1R antagonists have been shown to protect mice from CD95- and TNF-α-mediated liver damage (9). As a direct outgrowth of the present study, since a number of neuroendocrine factors regulate biliary functions by autocrine mechanisms, we propose to evaluate the possible autocrine role of SP in the growth and damage of the biliary epithelium.

ACKNOWLEDGMENTS

We acknowledge Bryan Moss, Scott & White, Medical Illustration Department for assistance with figures, and the Scott & White Hospital animal facility staff assistance with animal surgical models. We thank Anna Webb and the Texas A&M Health Science Center Microscopy Imaging Center for assistance with confocal microscopy.

GRANTS

This work was supported by the Dr. Nicholas C. Hightower Centennial Chair of Gastroenterology to Dr. Alpini from Scott & White Hospital, a Veterans Affairs (VA) Research Scholar Award, a VA Merit Award, and the National Institute of Diabetes and Digestive and Kidney Diseases (NIDDK) Grant DK062975 to Dr. Alpini. Portions of this study were supported by *1*) by a Scott & White grant award (no. 060483) from Scott & White and the NIDDK RO1 Grant (DK081442) to Dr. Glaser and *2*) a grant from Health and Labor Sciences Research Grants for the Research on Measures for Intractable Diseases (from the Ministry of Health, Labor and Welfare of Japan) and from Grant-in Aid for-Scientific Research C (21590822) from Japan Society for the Promotion of Science to Y. Ueno.

DISCLOSURES

No conflicts of interest, financial or otherwise, are declared by the author(s).

REFERENCES

1. **Almeida TA, Rojo J, Nieto PM, Pinto FM, Hernandez M, Martin JD, Candenas ML.** Tachykinins and tachykinin receptors: structure and activity relationships. *Curr Med Chem* 11: 2045–2081, 2004.
2. **Alpini G, Glaser S, Robertson W, Rodgers RE, Phinizy JL, Lasater J, LeSage G.** Large but not small intrahepatic bile ducts are involved in secretin-regulated ductal bile secretion. *Am J Physiol Gastrointest Liver Physiol* 272: G1064–G1074, 1997.
3. **Alpini G, Glaser S, Ueno Y, Pham L, Podila PV, Caligiuri A, LeSage G, LaRusso NF.** Heterogeneity of the proliferative capacity of rat cholangiocytes after bile duct ligation. *Am J Physiol Gastrointest Liver Physiol* 274: G767–G775, 1998.
4. **Alpini G, Lenzi R, Sarkozi L, Tavoloni N.** Biliary physiology in rats with bile ductular cell hyperplasia. Evidence for a secretory function of proliferated bile ductules. *J Clin Invest* 81: 569–578, 1988.
5. **Alpini G, Prall RT, LaRusso NF.** The pathobiology of biliary epithelia. In: *The Liver: Biology & Pathobiology* (4th ed.), edited by Arias IM, Boyer JL, Chisari FV, Fausto N, Jakoby W, Schachter D, and Shafritz DA. Philadelphia, PA: Lippincott Williams & Wilkins, 2001, p. 421–435.
6. **Alpini G, Roberts S, Kuntz SM, Ueno Y, Gubba S, Podila PV, LeSage G, LaRusso NF.** Morphological, molecular, and functional heterogeneity of cholangiocytes from normal rat liver. *Gastroenterology* 110: 1636–1643, 1996.
7. **Alvaro D, Mancino MG, Glaser S, Gaudio E, Marzioni M, Francis H, Alpini G.** Proliferating cholangiocytes: a neuroendocrine compartment in the diseased liver. *Gastroenterology* 132: 415–431, 2007.
8. **Alvaro D, Onori P, Metalli VD, Svegliati-Baroni G, Folli F, Franchitto A, Alpini G, Mancino MG, Attili AF, Gaudio E.** Intracellular pathways

mediating estrogen-induced cholangiocyte proliferation in the rat. *Hepatology* 36: 297–304, 2002.

9. **Bang R, Biburger M, Neuhuber WL, Tiegs G.** Neurokinin-1 receptor antagonists protect mice from CD95- and tumor necrosis factor-alpha-mediated apoptotic liver damage. *J Pharmacol Exp Ther* 308: 1174–1180, 2004.
10. **Bang R, Sass G, Kiemer AK, Vollmar AM, Neuhuber WL, Tiegs G.** Neurokinin-1 receptor antagonists CP-96,345 and L-733,060 protect mice from cytokine-mediated liver injury. *J Pharmacol Exp Ther* 305: 31–39, 2003.
11. **Bendtsen F, Schifter S, Henriksen JH.** Increased circulating calcitonin gene-related peptide (CGRP) in cirrhosis. *J Hepatol* 12: 118–123, 1991.
12. **Bozic CR, Lu B, Hopken UE, Gerard C, Gerard NP.** Neurogenic amplification of immune complex inflammation. *Science* 273: 1722–1725, 1996.
13. **Charron L, Peyronnard JM, Marchand L.** Sensory neuropathy associated with primary biliary cirrhosis. Histologic and morphometric studies. *Arch Neurol* 37: 84–87, 1980.
14. **DeMorrow S, Glaser S, Francis H, Venter J, Vaculin B, Vaculin S, Alpini G.** Opposing actions of endocannabinoids on cholangiocarcinoma growth: recruitment of Fas and Fas ligand to lipid rafts. *J Biol Chem* 282: 13098–13113, 2007.
15. **Francis H, Franchitto A, Ueno Y, Glaser S, DeMorrow S, Venter J, Gaudio E, Alvaro D, Fava G, Marzioni M, Vaculin B, Alpini G.** H3 histamine receptor agonist inhibits biliary growth of BDL rats by down-regulation of the cAMP-dependent PKA/ERK1/2/ELK-1 pathway. *Lab Invest* 87: 473–487, 2007.
16. **Francis H, Glaser S, DeMorrow S, Gaudio E, Ueno Y, Venter J, Dostal D, Onori P, Franchitto A, Marzioni M, Vaculin S, Vaculin B, Katki K, Stutes M, Savage J, Alpini G.** Small mouse cholangiocytes proliferate in response to H1 histamine receptor stimulation by activation of the IP_3/CaMK I/CREB pathway. *Am J Physiol Cell Physiol* 295: C499–C513, 2008.
17. **Francis H, Glaser S, Ueno Y, LeSage G, Marucci L, Benedetti A, Taffetani S, Marzioni M, Alvaro D, Venter J, Reichenbach R, Fava G, Phinizy JL, Alpini G.** cAMP stimulates the secretory and proliferative capacity of the rat intrahepatic biliary epithelium through changes in the PKA/Src/MEK/ERK1/2 pathway. *J Hepatol* 41: 528–537, 2004.
18. **French BT, Lee WH, Maul GG.** Nucleotide sequence of a cDNA clone for mouse pro alpha 1(I) collagen protein. *Gene* 39: 311–312, 1985.
19. **Glaser S, Benedetti A, Marucci L, Alvaro D, Baiocchi L, Kanno N, Caligiuri A, Phinizy JL, Chowdhury U, Papa E, LeSage G, Alpini G.** Gastrin inhibits cholangiocyte growth in bile duct-ligated rats by interaction with cholecystokinin-B/gastrin receptors via D-myo-inositol 1,4,5-triphosphate-, $Ca^{(2+)}$-, and protein kinase C alpha-dependent mechanisms. *Hepatology* 32: 17–25, 2000.
20. **Glaser S, DeMorrow S, Wise C, Francis H, Venter J, Gaudio E, Kopriva S, Franchitto A, Ueno Y, Onori P, Carpino G, Alpini G.** The α1-adrenergic receptor agonist, phenylephrine, stimulates the proliferation of small mouse cholangiocytes by activation of the Ca^{2+}-dependent transcription factors, NFATc1 and NFATc4. *Hepatology* 50: 2009.
21. **Glaser S, Gaudio E, Rao A, Pierce LM, Onori P, Franchitto A, Francis HL, Dostal DE, Venter JK, DeMorrow S, Mancinelli R, Carpino G, Alvaro D, Kopriva SE, Savage JM, Alpini G.** Morphological and functional heterogeneity of the mouse intrahepatic biliary epithelium. *Lab Invest* 89: 456–469, 2009.
22. **Glaser S, Lam IP, Franchitto A, Gaudio E, Onori P, Chow BK, Wise C, Kopriva S, Venter J, White M, Ueno Y, Dostal D, Carpino G, Mancinelli R, Butler W, Chiasson V, DeMorrow S, Francis H, Alpini G.** Knockout of secretin receptor reduces large cholangiocyte hyperplasia in mice with extrahepatic cholestasis induced by bile duct ligation. *Hepatology* 52: 204–214, 2010.
23. **Glaser S, Ueno Y, DeMorrow S, Chiasson VL, Katki KA, Venter J, Francis HL, Dickerson IM, DiPette DJ, Supowit SC, Alpini G.** Knockout of alpha-calcitonin gene-related peptide reduces cholangiocyte proliferation in bile duct ligated mice. *Lab Invest* 87: 914–926, 2007.
24. **Hakanson R, Wang ZY, Folkers K.** Comparison of spantide II and CP-96,345 for blockade of tachykinin-evoked contractions of smooth muscle. *Biochem Biophys Res Commun* 178: 297–301, 1991.
25. **Holzer P.** Efferent-like roles of afferent neurons in the gut: blood flow regulation and tissue protection. *Auton Neurosci* 125: 70–75, 2006.
26. **Khawaja AM, Rogers DF.** Tachykinins: receptor to effector. *Int J Biochem Cell Biol* 28: 721–738, 1996.
27. **Laniyonu A, Sliwinski-Lis E, Fleming N.** Different tachykinin receptor subtypes are coupled to the phosphoinositide or cyclic AMP signal transduction pathways in rat submandibular cells. *FEBS Lett* 240: 186–190, 1988.
28. **Lazaridis KN, Strazzabosco M, LaRusso NF.** The cholangiopathies: disorders of biliary epithelia. *Gastroenterology* 127: 1565–1577, 2004.
29. **Lee FY, Lin HC, Tsai YT, Chang FY, Lu RH, Hou MC, Li CP, Chu CJ, Wang SS, Lee SD.** Plasma substance P levels in patients with liver cirrhosis: relationship to systemic and portal hemodynamics. *Am J Gastroenterol* 92: 2080–2084, 1997.
30. **LeSage G, Alvaro D, Benedetti A, Glaser S, Marucci L, Baiocchi L, Eisel W, Caligiuri A, Phinizy JL, Rodgers R, Francis H, Alpini G.** Cholinergic system modulates growth, apoptosis, and secretion of cholangiocytes from bile duct-ligated rats. *Gastroenterology* 117: 191–199, 1999.
31. **LeSage G, Glaser S, Marucci L, Benedetti A, Phinizy JL, Rodgers R, Caligiuri A, Papa E, Tretjak Z, Jezequel AM, Holcomb LA, Alpini G.** Acute carbon tetrachloride feeding induces damage of large but not small cholangiocytes from BDL rat liver. *Am J Physiol Gastrointest Liver Physiol* 276: G1289–G1301, 1999.
32. **Lillie RD, Ashburn LL.** Supersaturated solutions of fat stains in dilute isopropanol for demonstration of acute fatty degeneration not shown by Herxheimer's technique. *Arch Pathol* 36: 432–440, 1943.
33. **Mancinelli R, Onori P, Gaudio E, DeMorrow S, Franchitto A, Francis H, Glaser S, Carpino G, Venter J, Alvaro D, Kopriva S, White M, Kossie A, Savage J, Alpini G.** Follicle-stimulating hormone increases cholangiocyte proliferation by an autocrine mechanism via cAMP-dependent phosphorylation of ERK1/2 and Elk-1. *Am J Physiol Gastrointest Liver Physiol* 297: G11–G26, 2009.
34. **Min BH, Foster DN, Strauch AR.** The 5′-flanking region of the mouse vascular smooth muscle alpha-actin gene contains evolutionarily conserved sequence motifs within a functional promoter. *J Biol Chem* 265: 16667–16675, 1990.
35. **Miyoshi H, Rust C, Roberts PJ, Burgart LJ, Gores GJ.** Hepatocyte apoptosis after bile duct ligation in the mouse involves Fas. *Gastroenterology* 117: 669–677, 1999.
36. **Mizuta K, Gallos G, Zhu D, Mizuta F, Goubaeva F, Xu D, Panettieri RA ,Jr, Yang J, Emala CW ,Sr.** Expression and coupling of neurokinin receptor subtypes to inositol phosphate and calcium signaling pathways in human airway smooth muscle cells. *Am J Physiol Lung Cell Mol Physiol* 294: L523–L534, 2008.
37. **Narumi S, Maki Y.** Stimulatory effects of substance P on neurite extension and cyclic AMP levels in cultured neuroblastoma cells. *J Neurochem* 30: 1321–1326, 1978.
38. **Patacchini R, De Giorgio R, Bartho L, Barbara G, Corinaldesi R, Maggi CA.** Evidence that tachykinins are the main NANC excitatory neurotransmitters in the guinea-pig common bile duct. *Br J Pharmacol* 124: 1703–1711, 1998.
39. **Taffetani S, Glaser S, Francis H, DeMorrow S, Ueno Y, Alvaro D, Marucci L, Marzioni M, Fava G, Venter J, Vaculin S, Vaculin B, Lam IP, Lee VH, Gaudio E, Carpino G, Benedetti A, Alpini G.** Prolactin stimulates the proliferation of normal female cholangiocytes by differential regulation of Ca^{2+}-dependent PKC isoforms. *BMC Physiol* 7: 6, 2007.
40. **Tahan V, Avsar E, Karaca C, Uslu E, Eren F, Aydin S, Uzun H, Hamzaoglu HO, Besisik F, Kalayci C, Okten A, Tozun N.** Adrenomedullin in cirrhotic and non-cirrhotic portal hypertension. *World J Gastroenterol* 9: 2325–2327, 2003.
41. **Trevenzoli IH, Rodrigues AL, Oliveira E, Thole AA, Carvalho L, Figueiredo MS, Toste FP, Neto JF, Passos MC, Lisboa PC, Moura EG.** Leptin treatment during lactation programs leptin synthesis, intermediate metabolism, and liver microsteatosis in adult rats. *Horm Metab Res* 42: 483–490, 2010.
42. **Trivedi M, Bergasa NV.** Serum concentrations of substance P in cholestasis. *Ann Hepatol* 9: 177–180, 2010.
43. **Ueno T, Tanikawa K.** Intralobular innervation and lipocyte contractility in the liver. *Nutrition* 13: 141–148, 1997.
44. **Ueno Y, Alpini G, Yahagi K, Kanno N, Moritoki Y, Fukushima K, Glaser S, LeSage G, Shimosegawa T.** Evaluation of differential gene expression by microarray analysis in small and large cholangiocytes isolated from normal mice. *Liver Int* 23: 449–459, 2003.
45. **Uyama N, Geerts A, Reynaert H.** Neural connections between the hypothalamus and the liver. *Anat Rec A Discov Mol Cell Evol Biol* 280: 808–820, 2004.
46. **Xia X, Demorrow S, Francis H, Glaser S, Alpini G, Marzioni M, Fava G, LeSage G.** Cholangiocyte injury and ductopenic syndromes. *Semin Liver Dis* 27: 401–412, 2007.

Enhanced Replication of Hepatitis B Virus With Frameshift in the Precore Region Found in Fulminant Hepatitis Patients

Jun Inoue, Yoshiyuki Ueno, Yuta Wakui, Koji Fukushima, Yasuteru Kondo, Eiji Kakazu, Masashi Ninomiya, Hirofumi Niitsuma, and Tooru Shimosegawa

Division of Gastroenterology, Tohoku University Graduate School of Medicine, Sendai, Japan

Background. The genotype B of hepatitis B virus (HBV) was reported to associate with fulminant hepatitis (FH). We aimed to clarify the characteristics of HBV obtained from FH patients in an area of Japan where genotype B HBV is prevalent.

Methods. Using serum samples of 16 HBV-associated FH patients, partial HBV sequences were determined. The effects of HBV mutation/insertion/deletion were evaluated using an in vitro HBV replication system.

Results. Of the 16 HBV isolates, 31% belonged to subgenotype B1/Bj, 38% were subgenotype B2/Ba, and 31% were subgenotype C2/Ce. Notably, the single nucleotide insertion/deletion that resulted in a frameshift of the precore protein was found exclusively in 60% of B1/Bj strains. An in vitro study showed that all of the frameshift mutants had significantly higher amounts of HBV DNA than did the wild type. One of the isolates had a novel insertion of A between nucleotides 1900 and 1901, which resulted in a 3-nucleotide change within the Kozak sequence of the core protein and enhanced the core protein expression in vitro.

Conclusions. The frameshift insertion/deletion in the precore region enhanced HBV replication and might be associated with the development of FH by the subgenotype B1/Bj HBV.

Hepatitis B virus (HBV) is one of the most common viruses affecting the human health. It causes a spectrum of chronic liver diseases including chronic hepatitis, liver cirrhosis, and hepatocellular carcinoma. Acute HBV infection induces acute self-limited hepatitis or fulminant hepatitis (FH), and the pathogenesis leading to the development of fulminant hepatitis B (FHB) is still being investigated. Although enhanced replication of the virus [1, 2] and an exuberant immune response by the host [3] are considered to be the main pathogeneses, various issues are not fully understood.

HBV contains a 3.2-kb, circular, partially double-stranded DNA genome; according to the heterogeneity of the nucleotide sequence, at least 8 (A–H) genotypes [4, 5] and, tentatively, 2 new genotypes (I and J) [6, 7] are classified. HBV genotypes are considered to affect the liver disease outcome [8], and the association of genotype B or subgenotype B1/Bj with FH was reported from Japan [9–11]. It has also been reported that several HBV mutations, such as T1753V (not T), T1754V, A1762T/G1764A, G1862T, G1896A, G1899A, and A2339G, were associated with FH [9–12]. In particular, the mutation of G1896A in the precore region, which makes a stop codon and abrogates hepatitis B e antigen (HBeAg), has been well documented [13–15]. HBV with G1896A was reported to have high replication capacity in vitro [10, 16]. However, in general clinical settings, chronic hepatitis patients with HBV with G1896A, which is the main cause of seroconversion of HBeAg to antibody against HBeAg (HBeAb), have lower viral load [17]. The reason for this discrepancy has not yet been elucidated clearly.

A difference in worldwide geographic distribution of the HBV genotypes has been noted. Also, in Japan, where HBV of genotype C prevails, there is a difference

Received 14 January 2011; accepted 26 May 2011.

Potential conflicts of interest: none reported.

Presented in part: 61th annual meeting of the American Association for the Study of Liver Diseases, Boston, Massachusetts, 29 October–2 November 2010.

Correspondence: Yoshiyuki Ueno, MD, PhD, Division of Gastroenterology, Tohoku University Graduate School of Medicine, 1-1 Seiryo, Aoba-ku, Sendai 980-8574, Japan (yueno@med.tohoku.ac.jp).

The Journal of Infectious Diseases 2011;204:1017–25

0022-1899 (print)/1537-6613 (online)/2011/2047-0008$14.00

DOI: 10.1093/infdis/jir485

in the distribution: it is known that the percentage of genotype B is higher in the northeast area [18]. However, little is known about the virological features of HBV obtained from FH patients in this area. Therefore, we aimed to investigate the characteristics of HBV, especially those of genotype B, that cause FH in our hospital in northeast Japan.

METHODS

Serum Samples

From January 1996 to November 2010, 60 patients were admitted to our hospital for acute HBV infection. Of them, 15 (25%) were diagnosed with FH. As there was an HBV carrier who developed FH, a total of 16 serum samples from FH patients were used in this study. The diagnosis of FH was made based on the following findings: coma grade II or higher and a prothrombin time <40% developing within 8 weeks after onset.

Determination of HBV Partial Sequences

The partial sequences of HBV were determined as described previously [19] with modifications. To amplify the 396-nucleotide sequence in the S gene (nucleotides 272–667; the nucleotide numbers are in accordance with a genotype C HBV isolate of 3215 nucleotides [AB033550]), total DNA extracted from 50 μL of serum was subjected to nested polymerase chain reaction (PCR) with the primers described previously. To amplify the 255-nucleotide sequence in the core promoter/precore region (nucleotides 1673–1927), the first round of PCR was carried out with primers B015 (5'-CAC GTY GCA TGG ARA CCA CCG TGA-3' [Y = C or T; R = A or G]) and B008 (5'-GTC AGA AGG CAA AAA AGA GAG TAA CTC-3'), and the second round was carried out with primers B016 (5'-GTC TTR CAT AAG AGG ACT CTT GGA CT-3') and B007 (5'-AAA GAG AGT AAC TCC ACA GAA GCT CC-3'). The amplification products were sequenced on both strands directly on an ABI PRISM 3100 Genetic Analyzer (Applied Biosystems), located in the Biomedical Research Core of Tohoku University Graduate School of Medicine. Sequence analysis and evaluation of the epsilon (ϵ) signal stability, which was calculated as minimum free energy, were performed using Genetyx-Mac (Version 12.2.6; Genetyx Corp). The sequence data from the current report have been assigned to the GenBank/EMBL/DDBJ with the accession numbers AB602749–AB602759 (partial S region sequence) and AB602760–AB602770 (partial core promoter/precore sequence).

Construction of Plasmids

A plasmid containing the 1.3-fold HBV genome (nucleotide 1051-3215/1-1953) was constructed as described previously [20] using serum of a self-limited acute hepatitis patient (AH-2; accession number of the full-genome sequence, AB602818) with HBV of the subgenotype B1/Bj in our hospital. Because the isolate had a mutation of G1899A in the precore region, the mutation was converted to the wild-type nucleotide using Quick Change II-E Site-Directed Mutagenesis Kit (Stratagene) as described previously [20], and the clone was used as a subgenotype B1/Bj wild-type clone.

The wild clone was used as template to construct a clone with a mutation of G1896A, an insertion of A between nucleotides 1837 and 1838 (1838insA), a deletion of a single nucleotide at 1846 (1846del), or an insertion of A between nucleotides 1900 and 1901 (1901insA). A clone with 1901insA was used as the next template to introduce the additional mutation of T1855C. All constructs were sequenced to confirm the introduced mutation/insertion/deletion.

Cell Culture and Transfection

Human hepatoma HepG2 cells were cultured as described previously [20]. On the next day, after seeding cells in 24-well plates at 1.25×10^5 cells/well, 0.5 μg/well of plasmid DNA was transfected using FuGENE HD Transfection Reagent (Roche Diagnostics), and the culture supernatant and cells were collected 3 days later. For Southern blot analysis, cells were seeded in 6-well plates at 5.0×10^5 cells/well, and 1.5 μg/well of plasmid DNA was transfected. In this system, the transfection efficiency could be evaluated with the level of hepatitis B surface antigen (HBsAg) in the culture supernatant [20]. The experiments were performed at least in triplicate.

Assay of HBV Markers

Five microliters of the supernatant was treated with 5 units of DNase I (TaKaRa Bio) at 37°C for 2 hours to digest the input plasmid DNA in the culture supernatant, and the reaction was stopped with ethylenediaminetetraacetic acid. Then, total DNA was extracted with a QIAamp DNA Blood Mini Kit (QIAGEN GmbH), and the amount of HBV DNA was quantified with real-time PCR using a StepOnePlus Real Time PCR System (Applied Biosystems) [21]. HBsAg and HBeAg in 50 μL of the culture supernatant were assayed by enzyme-linked immunosorbent assay [20]. To detect the intracellular replicative intermediates of HBV, the core particle–associated HBV DNA in the cells was isolated as described previously [20]. After DNase I treatment for the removal of unprotected DNA, extracted total DNA was analyzed by Southern blotting using a full-length HBV DNA probe labeled with PCR DIG Probe Synthesis Kit (Roche Diagnostics).

In Vitro Cell-Free Protein Expression

To investigate whether the change of the Kozak sequence around the initiation codon of the core protein affects the protein expression, TNT T7 Quick for PCR DNA (Promega) was used. The template of transcription/translation was a purified PCR product that was amplified from the subgenotype B1/Bj wild clone. To make the wild-type template, PCR was performed with a forward primer CoreKW (5'-GGA TCC TAA TAC GAC TCA CTA TAG